JACS
JOURNAL OF THE AMERICAN CHEMICAL SOCIETY
pubs.acs.org/JACS
Article

Atomic Resolution Interactions Regulating Partitioning of a FUS Folded RRM Domain into Model CAPRIN1 Condensates

Rashik Ahmed,* Jeffrey P. Bonin, Julie D. Forman-Kay, and Lewis E. Kay*

Cite This: J. Am. Chem. Soc. 2025, 147, 33071−33085
Read Online
ACCESS | Metrics & More | Article Recommendations | Supporting Information

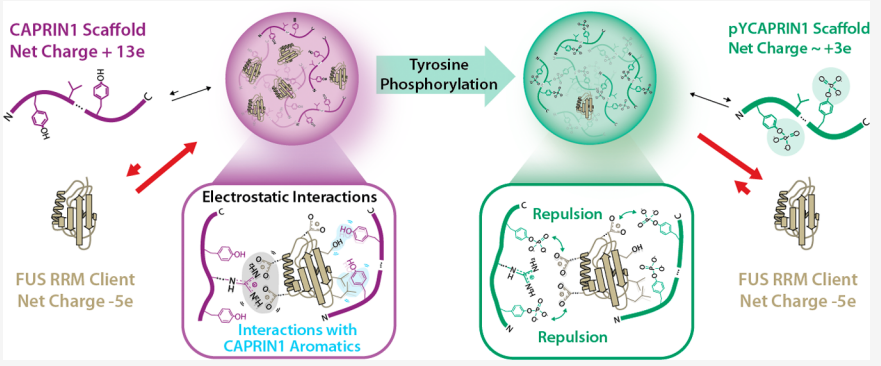

ABSTRACT: Biomolecular condensates enrich specific client molecules while excluding others, often modulating conformational landscapes, and hence functions, of molecules dissolved within them. NMR-based atomic resolution studies have focused on interactions between scaffold proteins and the unfolded states of client proteins to understand the factors that influence client partitioning into condensed phases. However, characterization of interactions involving the folded client conformer is required to obtain a complete picture of how dissolution within the condensed phase affects the client energy landscape. Here, we use solution NMR spectroscopy to investigate, at atomic resolution, the interactions mediating the selective partitioning of a folded client, the FUS RNA Recognition Motif (RRM), into condensates formed by the scaffold protein CAPRIN1. At 40 °C, approximately 40% of FUS RRM remains folded in the CAPRIN1 condensed phase and high-resolution [^{1}H−^{15}N]-HSQC spectra can be recorded, enabling site-specific interactions between the folded client and scaffold to be mapped across the entire FUS RRM sequence. Using intermolecular NOE and PRE (mixed solutions), and chemical shift perturbation (demixed solution) analyses, we identify a set of interaction surfaces on the folded FUS RRM that enable multiple contacts with aromatic- and arginine-rich regions of CAPRIN1. These heterotypic interactions lead to a 30-fold enrichment of FUS RRM within the condensate and overlap with sites responsible for CAPRIN1 homotypic phase separation, suggesting a shared molecular basis for scaffold-scaffold and scaffold-client recognition. Notably, tyrosine phosphorylation of CAPRIN1 disrupts these interactions and reduces client partitioning by over 2 orders of magnitude, highlighting how post-translational modifications can profoundly regulate condensate composition.

INTRODUCTION

Eukaryotic cells are well-known to be organized by membrane-bound compartments, providing spatial control over biochemical processes that are necessary for their survival. However, organization can also be achieved by the formation of nonmembrane-delimited compartments referred to as biomolecular condensates.[1,2] Condensates are often formed through the process of phase separation, whereby dynamic, multivalent interactions between scaffolding molecules drive the formation of two or more coexisting phases, including a scaffold-depleted (dilute) phase and a scaffold-rich (condensed) phase.[3,4] The high concentrations of scaffold molecules in the condensed phase create a unique solvent environment that selectively enriches a subset of biomolecules, *i.e.*, clients.[1] Depending on the sequence and chemical features of condensate scaffolds, distinct pools of clients are recruited to the condensate, where their energy landscapes, and hence functions, can be significantly affected.[5−7] Changes to scaffold chemical groups, such as through post-translational modifications or pH shifts that alter histidine charge, can dynamically modulate condensate composition.[8] Through such compositional control, condensates can regulate the biochemical processes that occur within them. In this context, understanding the physics of the interactions between scaffold and

Received: June 27, 2025
Revised: August 6, 2025
Accepted: August 7, 2025
Published: August 26, 2025

ACS Publications
© 2025 American Chemical Society

https://doi.org/10.1021/jacs.5c10918
J. Am. Chem. Soc. 2025, 147, 33071−33085

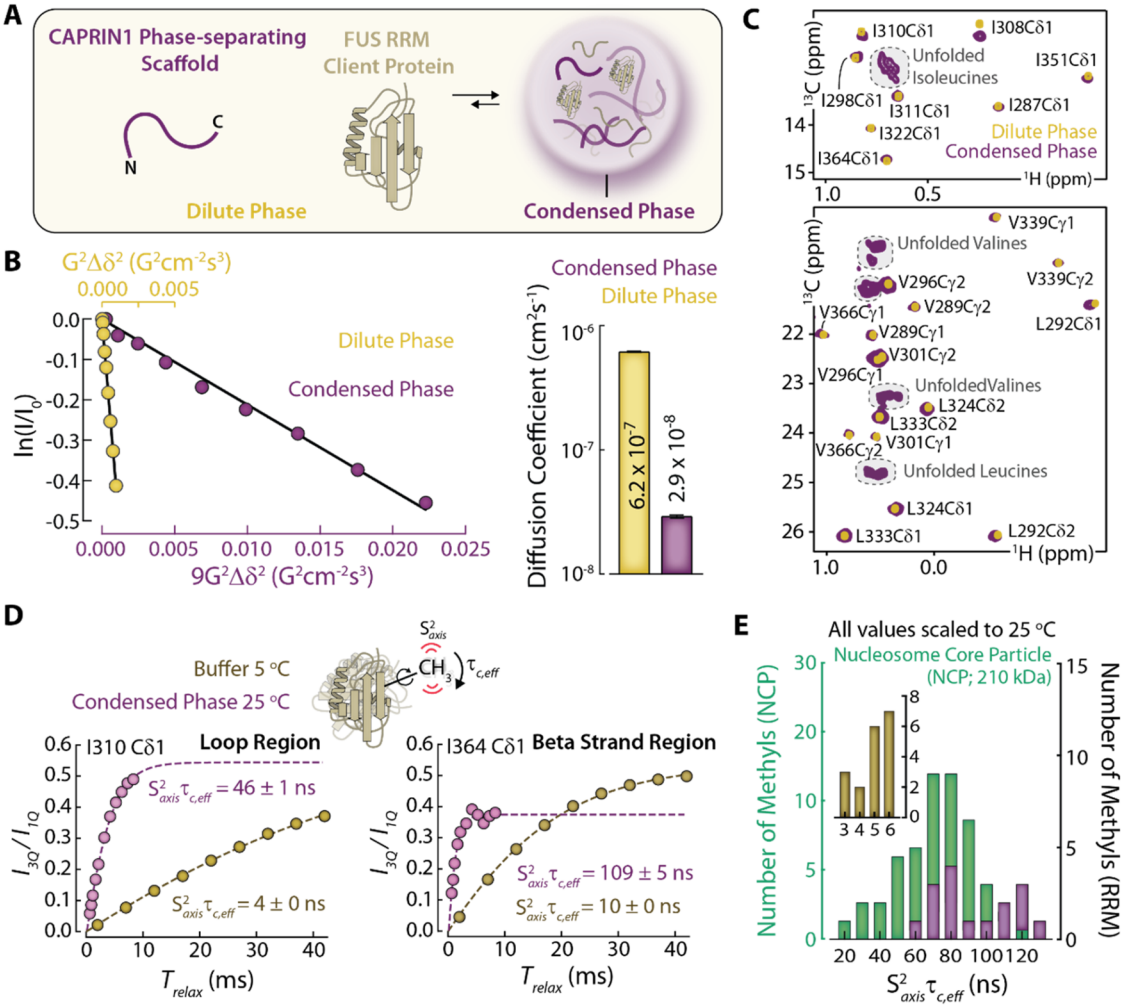

Figure 1. The CAPRIN1 condensate, 25 °C, presents a highly viscous environment for the folded FUS RRM. (A) Schematic depicting the FUS RRM folded client protein and CAPRIN1 phase-separating scaffold used in this study. (B) Measurements of CAPRIN1 diffusion constant (25 °C) in dilute (*yellow*) and condensed (*purple*) phases using single (dilute phase) and triple (condensed phase) quantum-based pulse field gradient experiments. The experimental data (points) were fit (solid lines) to obtain diffusion coefficients (*right*), as described in Material and Methods. (C) ^{1}H,^{13}C delayed decoupling methyl-TROSY spectra of ^{2}H, ^{15}N, ^{13}C-ILV FUS RRM in dilute (*yellow*) and condensed (*purple*) phases recorded at 800 MHz, 25 °C. Signals derived from unfolded FUS conformers are indicated by the gray highlighted regions. (D) (*inset*) Cartoon diagram highlighting side chain methyl group dynamics on the ps-ns time scale; the product $S^2_{Axis}\tau_{c,eff}$ is obtained in NMR relaxation measurements. Qualitatively, S^2_{Axis} is related to the amplitude of motion of the 3-fold methyl symmetry axis and $\tau_{c,eff}$ is a methyl-specific correlation time characterizing the tumbling of the methyl axis. Plots of experimental ratios of differences (I_{3Q}) and sums (I_{1Q}) of single quantum methyl ^{1}H magnetization vs. relaxation delay (T_{relax}) for selected residues from the loop (*left*) and beta-strand (*right*) regions of FUS RRM in buffer (*brown*) and in the CAPRIN1 condensed phase (*purple*). (E) Histogram of $S^2_{Axis}\tau_{c,eff}$ values for the 10.4 kDa FUS RRM in buffer (*brown*; inset) and in CAPRIN1 condensed phase (*purple*), where only methyl groups from folded regions of the FUS RRM are included, and for the 210 kDa nucleosome core particle (NCP, *green*) in buffer (25 °C). Only residues in the folded cores of each histone (data from all four histones are included in the analysis) were used in the comparison, with loops and disordered tails excluded. Notably, slightly larger values for the folded FUS RRM in the condensed phase are obtained than for the NCP in buffer. Measurements on NCP and FUS RRM samples in buffer were carried out at 37 °C and 5 °C, respectively, with reported $S^2_{Axis}\tau_{c,eff}$ values in panel E scaled to 25 °C (see Methods).

client molecules that are responsible for the solvation and recruitment of clients into condensates is an important, but currently under-studied, area of investigation.

Solution NMR spectroscopy is a particularly valuable tool for studies of phase separation when the scaffold molecules are intrinsically disordered or contain large regions of disorder.[9] While the liquid-like properties and highly dynamic nature of these condensates challenge other atomic resolution techniques, NMR is ideally suited to explore both the structures and the dynamics of the scaffold proteins and the intermolecular interactions that stabilize them in the condensate. Not surprisingly, most solution NMR studies of phase separation have focused on condensates comprised of dynamic scaffold proteins.[10−18] These proteins are present at high concentrations, and their significant motions compensate for the condensates' viscous nature, so that high resolution spectra can be recorded.

NMR studies of client molecules in condensates, in particular those that are folded, are more challenging in comparison to applications focused on disordered scaffold proteins. First, clients are present at concentrations that are significantly reduced relative to the surrounding scaffold, by as much as 2 orders of magnitude in many of our applications.[5,19,20] In addition to sensitivity issues, this

https://doi.org/10.1021/jacs.5c10918
J. Am. Chem. Soc. 2025, 147, 33071−33085

concentration imbalance obscures the client peaks of interest unless the intense scaffold resonances are suppressed, such as by using coherence transfer pulsed field gradient approaches.[21] Second, folded client proteins tumble slowly in the viscous condensate environment, and without the segmental backbone dynamics of their disordered counterparts NMR signals tend to relax rapidly. Accordingly, correlations are often not observed from the folded client in conventional [^{1}H−^{15}N]-HSQC spectra.[5] In contrast, high quality [^{1}H−^{13}C]-methyl-TROSY spectra can be recorded on deuterated, methyl-protonated samples using a delayed-decoupling strategy that we have described previously to obtain site-specific information for methyl-bearing amino acids.[21] Yet, having reporters for every residue in a protein, as would be the case in amide correlation spectroscopy, remains an important objective for obtaining a comprehensive understanding of the client-scaffold interactions governing client recruitment into condensates.

In this work, we explore experimental conditions under which amide correlation spectroscopy of folded client proteins within condensates is feasible using a model client-scaffold system composed of the 95 amino acid client RNA Recognition Motif (RRM) from the Fused in Sarcoma (FUS) stress granule protein dissolved in a condensate scaffolded by the C-terminal 101 residues from the stress granule protein Cell Cycle Associated Protein 1 (CAPRIN1) (referred to as CAPRIN1 in what follows) (Figure 1A). Our previous studies of the FUS RRM:CAPRIN1 system using ^{1}H−^{15}N based NMR spectroscopy have focused on interactions between the intrinsically disordered CAPRIN1 scaffold and the unfolded ensemble of FUS RRM.[20] However, while the FUS RRM folding/unfolding equilibrium is shifted toward the unfolded state in the highly CAPRIN1 concentrated (∼30 mM) condensed phase environment, the folded state remains significantly populated (∼70 and 40% at 25 and 40 °C, respectively[20]). A complete understanding of how the energy landscape of FUS RRM is affected by the condensate requires atomic resolution characterization of the interactions between the folded client and scaffold as well. Nevertheless, such interactions are difficult to quantify in the case of folded clients, as discussed above.

Here we have exploited the steep temperature dependence of condensate viscosity to identify a temperature that sufficiently reduces the overall viscosity of the condensate environment so that amide correlations from the folded RRM client can be detected. Initial studies at 25 °C, using methyl-based relaxation experiments recorded on deuterated, Ile/Leu/Val (ILV)-methyl labeled FUS RRM in a CAPRIN1 condensate, establish that the FUS RRM effective tumbling time is comparable to that of a 210 kDa particle in buffer, explaining why amide correlations from the folded FUS RRM state are not observed in studies at this temperature. However, at 40 °C, where there is a significant reduction in the overall viscosity of the condensate environment, it is possible to detect amide correlations from the folded RRM client. Combined with optimized sample deuteration and selective isotopic labeling strategies for condensed phase measurements, in concert with intermolecular Paramagnetic Relaxation Enhancement (PRE) and Nuclear Overhauser Effect Spectroscopy (NOESY) in mixed solutions, it thus becomes possible to map folded client-scaffold interaction sites. These include the N-terminal negatively charged region spanning D276−T286, the C-terminal ends of the α1 (∼Q307-I310) and α2 (∼A350-G361) helices, as well as several small patches such as ∼L324-T326 and ∼F368-T370 of FUS RRM. Intermolecular interactions, as probed through PREs read-out on FUS RRM, are strongest when originating from aromatic-rich segments of CAPRIN1 and diminish with increasing buffer ionic strength, indicating contributions from both aromatic and electrostatic interactions. Consistent with these observations, FUS RRM interaction sites map to aromatic-rich, and to a lesser extent arginine-rich, regions of CAPRIN1. Notably, phosphorylation of CAPRIN1 Tyr residues, which simultaneously modulates the net charge of the CAPRIN1 chain and the chemical properties of the Tyr side chains, reduces FUS RRM partitioning into CAPRIN1 condensates by over 2 orders of magnitude. Collectively, these findings expand our understanding of the molecular interactions governing recruitment of folded client proteins into condensates. They also highlight how post-translational modifications can modulate these interactions to alter client partitioning, pointing to a dynamic mechanism by which cells can regulate condensate composition in response to physiological signals or stress.

METHODS

Expression and Purification of CAPRIN1 and FUS RRM. The human CAPRIN1 (S607-Q707) and FUS RRM (D276-T370) sequences were subcloned into pET-His-SUMO vectors. The FUS RRM construct harbored an N-terminal diglycine (GG) for efficient cleavage of the His-SUMO solubility tag while the CAPRIN1 construct contained the mutations N623T, N630T, V610A and L621A. Substitution of Asn to Thr eliminated the formation of Iso-Asp linkages that would otherwise occur over time, as discussed previously,[14] while removal of Val and Leu residues ensured that methyl signals from the FUS RRM client are unobstructed by peaks derived from CAPRIN1[21] (there are no Ile residues in CAPRIN1). Both FUS RRM and CAPRIN1 vectors were transformed into *Escherichia coli* BL21 (DE3) RIPL cells and grown to an OD_{600}∼0.6−0.8, after which protein expression was induced with 0.5 mM IPTG and allowed to continue overnight at 18 °C. Cells harboring the CAPRIN1 plasmid were grown in LB for production of unlabeled protein. Deuterated, ILV-labeled FUS RRM was produced by growing RIPL cells in M9 D_2O media supplemented with 3 g/L d_7-glucose as well as 100 mg/L of 2-keto-3-methyl-d_3-3-d_1-4-^{13}C-butyrate (for nonstereospecific labeling of Leu, Val-$^{13}CH_3/^{12}CD_3$) and 60 mg/L of 2-keto-3-d_2-4-^{13}C-butyrate (for $^{13}CH_3$ labeling of Ileδ1) added 1 h prior to the induction of protein expression.

Cells were harvested via centrifugation, resuspended in lysis buffer, and sonicated for 15 min (2 s on, 2 s off). The lysis buffer for CAPRIN1 contained 6 M guanidinium hydrochloride, 50 mM Tris pH 8, 500 mM NaCl and 10 mM Imidazole, while the FUS RRM lysis buffer contained 50 mM Tris pH 8, 300 mM NaCl, and 20 mM imidazole, supplemented with lysozyme, RNase A (Roche), and a protease inhibitor cocktail tablet (Roche). Lysed cells were spun down at 13,800 g for 1 h, and the supernatant was loaded onto a Ni-NTA column (GE Healthcare) equilibrated with lysis buffer. The column was washed extensively with lysis buffer and the proteins were eluted with a solution of 50 mM Tris pH 8, 150 mM NaCl, 400 mM imidazole. The His-SUMO tag was cleaved with HisSUMO protease while exchanging against 50 mM Tris pH 8, 150 mM NaCl, 10 mM imidazole, 2 mM β-mercaptoethanol buffer (and 10% glycerol in the case of FUS RRM) at 4 °C. The cleaved proteins were loaded onto a Ni-NTA column to remove the His-SUMO tag and HisSUMO protease, concentrated, and injected onto a Superdex75 (26/600) column equilibrated with either 3 M guanidinium hydrochloride, 50 mM Tris pH 8 or 50 mM Tris pH 8, 10% glycerol for CAPRIN1 and FUS RRM, respectively. The purified protein fractions were pooled and stored at −20 °C until use.

Incorporation of Dia- and Paramagnetic Metal-Bound Cages onto CAPRIN1. Maleimido-monoamide-DOTA (Macrocyclics, B-272) was obtained as a powder and dissolved in 4 M

https://doi.org/10.1021/jacs.5c10918
J. Am. Chem. Soc. 2025, 147, 33071−33085

guanidinium hydrochloride with 50 mM Tris pH 7 buffer to a final concentration of 100 mM. Cysteine residues were individually introduced into CAPRIN1 (residues 607-707), which lacks native cysteines, in the background of the N623T, N630T, V610A, and L621A mutations. The specific cysteine substitutions used were S615C and A658C (one per construct). Each cysteine mutant (~50 μM) was reacted with a 5-fold molar excess of DOTA cage overnight at 37 °C in 4 M guanidinium hydrochloride, 50 mM Tris pH 7, and 1 mM TCEP. Completion of the labeling reaction was confirmed by mass spectrometry. The DOTA-labeled CAPRIN1 variants were then split into two equal aliquots, to which either gadolinium(III) chloride or lutetium(III) chloride was added in 50-fold molar excess. After a second overnight incubation at 37 °C, the samples were buffer-exchanged using a HiPrep 26/10 desalting column pre-equilibrated with NMR buffer to remove unbound metal ions and excess DOTA cage.

Preparation of FUS RRM:CAPRIN1 Condensed Phase (Figures 1, 2, and 3A). The FUS RRM:CAPRIN1 condensed phase was prepared according to the protocol schematically depicted in Figure S1. Unlabeled CAPRIN1 and ^{2}H, ^{15}N, ^{13}C-ILV FUS RRM were buffer-exchanged into a solution of 20 mM MES pH 6.0, 0.5 mM EDTA using a HiPrep 26,10 Desalting column and concentrated. A 1 mL mixture was prepared by combining 280 μL of 1 mM FUS RRM and 720 μL of 11 mM CAPRIN1 on ice. After equilibration for 30 min, phase separation was induced by diluting the FUS RRM:CAPRIN1 mixture 10% with 20 mM MES pH 6.0, 2 M NaCl, 0.5 mM EDTA, 100% D_2O, resulting in a final NaCl concentration of 200 mM and 10% D_2O. A portion of the phase-separated mixture was transferred into a 3 mm NMR tube and stored at 4 °C until the droplets merged into a homogeneous condensed phase and settled at the bottom of the tube. The dilute phase was then decanted, replaced with more of the phase-separated mixture, and subjected to another cooling and droplet fusion cycle. This procedure was repeated until the condensed phase volume was sufficient to fill the entire NMR receiver coil, with the dilute phase remaining on top. The sample was equilibrated to the measurement temperature (25 or 40 °C) for approximately 8 h before NMR experiments. After completing the condensed phase NMR measurements at each temperature, a portion of the dilute phase above was decanted into a separate 3 mm NMR tube to generate the dilute phase samples used in this study.

Details pertaining to the preparation of phase-separated solutions for measuring FUS RRM partition coefficients are provided below in the section titled "*2D [^{1}H, ^{13}C]-HSQCs for determining CAPRIN1 and pYCAPRIN1 condensed phase concentrations and partition coefficients of FUS RRM in phase-separated CAPRIN1 and pYCAPRIN1 solutions (Figure 5; 600 MHz)*".

NMR Measurements. NMR spectra were acquired on one of either 23.5 T (1 GHz ^{1}H frequency; Bruker Avance Neo), 18.8 T (800 MHz ^{1}H frequency; Bruker Avance III HD), or 14.0 T (600 MHz ^{1}H frequency; Bruker Avance III HD) spectrometers, all equipped with cryogenically cooled *x*, *y*, *z* pulsed-field gradient triple-resonance probes. Spectra were processed using NMRPipe[22] and analyzed with either peakipy (https://github.com/j-brady/peakipy) or NMRFAM-SPARKY.[23]

Single Quantum and Triple Quantum Pulsed-Field Gradient NMR for Measurement of CAPRIN1 Diffusion Constants in FUS RRM:CAPRIN1 Dilute and Condensed Phases (Figures 1B, 2A; 800 MHz). CAPRIN1 diffusion measurements in the dilute phase were performed using a single quantum, stimulated-echo based pulse scheme described previously,[24] with the exception that ^{15}N and ^{13}C pulses were interchanged. Diffusion constants were obtained by integrating the CAPRIN1 methionine ^{1}H signals in 1D experiments, recorded as a function of encoding/decoding gradient strengths, each applied as a bipolar gradient pair. The length of each of the encoding and decoding gradients was 1.0 ms for a total time δ of 2.0 ms, with a diffusion delay (Δ) of 150 ms. Condensed phase diffusion constants of CAPRIN1 were obtained using a triple quantum-based pulse scheme.[25] Diffusion measurements conducted at 25 °C were recorded with Δ = 150 ms and lengths of encoding/decoding gradients (δ) totaling 3.2 ms while 40 °C measurements were recorded with Δ = 150 ms and encoding/decoding gradients totaling 1.6 ms. Diffusion measurements were recorded on a Bruker 800 MHz spectrometer (maximum gradient strength of 44.6 G/cm). Experiments were recorded using 3 mm NMR tubes and repeated with different Δ values to ensure the absence of convection. Phase-separated sample preparation was as described above.

Measuring FUS RRM Methyl $S^2_{Axis}\tau_c$ Values in Buffer and in the FUS RRM:CAPRIN1 Condensed Phase (Figure 1D,E; 800 MHz). FUS RRM methyl $S^2_{Axis}\tau_c$ values in buffer and CAPRIN1 condensed phase (prepared as described above) were obtained as described previously[24] using an approach in which the sums (I_{SQ}) and differences (I_{3Q}) of single quantum methyl ^{1}H magnetization components are quantified. Condensed phase measurements were conducted at 25 °C, 800 MHz using 11 delays (0.5, 0.75, 1, 1.5, 2, 3, 4, 5, 6, 7, 8) ms with 32 and 144 scans for measuring I_{SQ} and I_{3Q}, respectively, for a total measurement time of ~6 days. Measurements in buffer were performed at 5 °C, 800 MHz using 9 delays (2, 7, 12, 17, 22, 27, 32, 37, 42) ms with 16 and 24 scans for measuring I_{SQ} and I_{3Q}, respectively, for a total measurement time of 1 day 10 h. $S^2_{Axis}\tau_c$ values of FUS RRM and nucleosome core particle (NCP) in buffer[26] were scaled to 25 °C based on the dependence of τ_c on temperature and viscosity. The histogram of the $S^2_{Axis}\tau_c$ values (25 °C) for NCP and FUS RRM in buffer and condensed phase was constructed with a bin width of 10 ns (Figure 1E).

[^{1}H,^{15}N] TROSY-HSQC Spectra of FUS RRM in Dilute and Condensed Phases of FUS RRM:CAPRIN1 (Figures 2B, 3A; 800 MHz). [^{1}H,^{15}N] TROSY-HSQC spectra of FUS RRM in the CAPRIN1 condensed phase (prepared as described above) were acquired at 25 °C on an 800 MHz spectrometer with an interscan delay of 1.5s, 128 scans/FID, ^{1}H and ^{15}N spectral widths and acquisition times of 15.0 and 30.0 ppm, and 64 and 35 ms, respectively, for a total acquisition time of 9 h and 54 min. ^{1}H and ^{15}N pulses were centered on the water line and 118 ppm, respectively. The condensed phase spectrum recorded at 40 °C was acquired with the same spectral widths and acquisition times and 456 scans/FID, for a total acquisition time of 1 day and 11 h. The corresponding 40 °C dilute phase spectrum was recorded with 8 scans/FID, for a total acquisition time of 37 min.

^{15}N-$R_{1\rho}$, ^{15}N-R_1, and Steady State ^{15}N{^{1}H}-NOE Measurements for Probing the Dynamics of Folded FUS RRM in Buffer and FUS RRM:CAPRIN1 Condensed Phases (Figure 2; 800 MHz). ^{15}N R_1 and $R_{1\rho}$ rates of ^{2}H,^{15}N,^{13}C-ILV FUS RRM were recorded in buffer and condensed phases of FUS RRM:CAPRIN1 (prepared as described above) using TROSY-HSQC based experiments, 40 °C, 800 MHz.[27] ^{15}N R_1 ($R_{1\rho}$) measurements in buffer were collected with a series of five (eight) time points extending from 10−700 ms (5−85 ms). Condensed phase ^{15}N R_1 ($R_{1\rho}$) measurements were collected with two (three) time points of 10 and 500 ms (2, 8, 16 ms). ^{15}N R_2 values were calculated using the following relationship:

$$R_2 = (R_{1\rho} - R_1 \cos^2 \vartheta)/\sin^2 \vartheta \quad (1)$$

where ϑ = arctan(v1/$\Delta\Omega$), v1 is the spin-lock field strength (2 kHz), and $\Delta\Omega$ is the offset (Hz) of the spin in question from the ^{15}N carrier.[28]

^{15}N{^{1}H}-heteronuclear NOEs of FUS RRM in buffer were obtained from a pair of experiments recorded either with a prescan delay of 8 s followed by saturation for 6 s or a delay of 14 s, as described previously.[29]

The FUS RRM diffusion tensor was estimated from amide R_2, R_1, and NOE values using the ROTDIF software package.[30] Only residues that (1) have a ^{15}N{^{1}H}-NOE > 0.74, and (2) lack a noticeable exchange contribution to R_2 based on the Bracken method[31] *i.e.*, their R_1 R_2 values do not significantly deviate from the mean of all rigid residues, (n = 43) were included in the analysis. For the isotropic diffusion tensor model a rotational correlation time $\tau_c = \frac{1}{6D_{iso}} = 4.55 \pm 0.01$ ns was obtained. This analysis was repeated with the Modelfree software[32] using the same amides, fixing S^2_s = 0.95, S^2_f = 1.0, and τ_s = 0 ps. This yielded an essentially identical value for τ_c

https://doi.org/10.1021/jacs.5c10918
J. Am. Chem. Soc. 2025, 147, 33071−33085

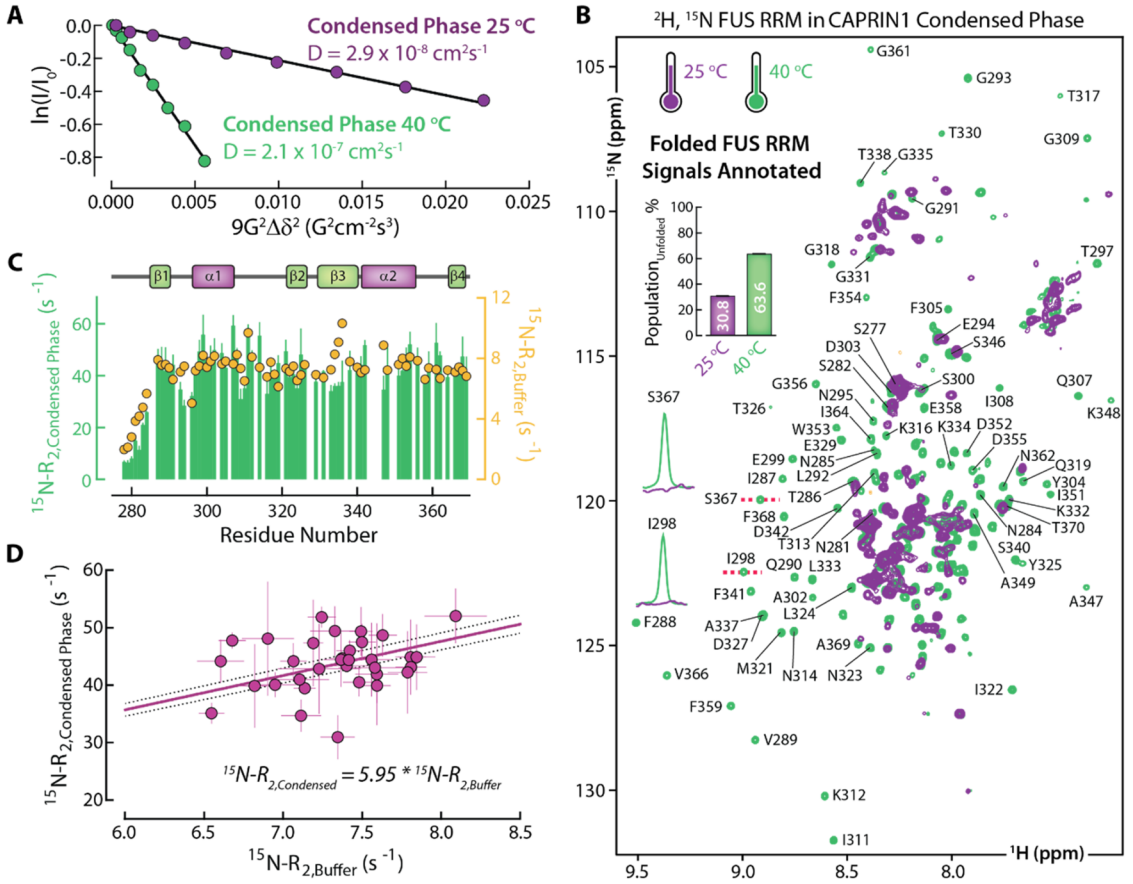

Figure 2. Steep temperature-dependence of condensed phase solution viscosity enables observation of folded FUS RRM signals in ^{1}H, ^{15}N correlation spectra at 40 °C. (A) Measurements of CAPRIN1 diffusion constants in the condensed phase at 25 °C (*purple*) and 40 °C (*light green*) using triple quantum-based pulse field gradient experiments. The experimental data (points) were fit (solid lines) to obtain diffusion coefficients, as described in Material and Methods. (B) Overlay of [^{1}H,^{15}N]-TROSY-HSQC spectra of ^{2}H, ^{15}N FUS RRM in the CAPRIN1 condensed phase at 25 °C (*purple*) and 40 °C (*light green*), measured at 800 MHz. Signals from folded FUS RRM are annotated in black. Slices through the ^{1}H dimension are provided for S367 and I298, highlighting the absence of signals from the folded conformer at 25 °C. Note that signals from CAPRIN1 (0.3% ^{15}N) and unfolded FUS RRM are also observed, but these do not interfere with peaks from the folded FUS RRM. Populations of unfolded FUS RRM states are indicated at both 25 and 40 °C, quantified as described elsewhere.[20] (C) Overlay of ^{15}N-R$_2$ profiles for FUS RRM in buffer (*yellow circles*) and in FUS RRM:CAPRIN1 condensed phase (*green bars*). FUS RRM domain architecture is schematically illustrated above. (D) Correlation between the ^{15}N-R$_2$ profiles shown in (C), focusing on rigid residues *i.e.* residues with steady state NOEs > 0.74 (buffer) that are not exhibiting μs-ms exchange.[31] Solid and dashed lines indicate the line of best fit and 90% confidence interval, respectively.

= 4.56 ± 0.01 ns. The "isotropic" correlation time was used to calculate the overall tumbling time of FUS RRM in the CAPRIN1 condensed phase, using relations indicated in Figure 2D and in the text.

$^{1}H^{N}$ R_2 Measurements of CAPRIN1:FUS RRM Interactions in Mixed Solutions via the Paramagnetic Relaxation Enhancement (PRE) Effect (Figure 3; 800 MHz). Amide proton R$_2$ relaxation rates were measured at 800 MHz, 25 °C, on samples containing 200 μM ^{15}N, ^{13}C FUS RRM and 200 μM ^{14}N CAPRIN1 conjugated with a DOTA cage coordinating either gadolinium (paramagnetic) or lutetium (diamagnetic) in 20 mM MES pH 6, 5% D$_2$O buffer. Measurements were recorded on samples with the metal-bound DOTA cage introduced at either position 615 or 658 of CAPRIN1, with the former remeasured in the presence of 150 mM NaCl. A gradient enhanced [^{1}H,^{15}N]-HSQC pulse scheme was used to measure amide proton R$_2$ relaxation rates with a ^{1}H spin−echo variable delay (−τ−selective 180°−τ−) inserted immediately prior to acquisition.[33] Homonuclear *J*-coupled evolution involving aliphatic and amide proton spins was refocused by applying a selective 180° REBURP[34] pulse positioned at the center of the amides during the middle of the ^{1}H spin−echo delay. Spectra were acquired with 4 scans/FID and ^{15}N t_1 acquisition times of 50 ms, for a total acquisition time of 3 h and 33 min/spectrum. Eight relaxation delays (T_{relax}) ranging either from 2−17.5 ms or 2−30 ms were used, as needed to sufficiently sample the decay of magnetization for the various samples. For each relaxation delay, the ratio of peak intensities in spectra recorded on paramagnetic and diamagnetic samples (I_{para}/I_{dia}) was computed. The paramagnetic relaxation enhancement effect was quantified by fitting the I_{para}/I_{dia} as a function of T_{relax} to an exponential decay function $I(t) = I_0 e^{-R_2 T_{relax}}$.

2D [^{1}H,^{15}N]-HSQC-Based NOE Experiments for Mapping Intermolecular FUS RRM-CAPRIN1 Interactions in Mixed Solutions (Figures 3, 4; 800 MHz and 1 GHz). To identify FUS RRM amide sites that interact with CAPRIN1 aromatic side chains, a mixed solution sample was prepared with 0.9 mM ^{1}H,^{13}C,^{14}N-labeled CAPRIN1 and 0.7 mM ^{2}H,^{12}C,^{15}N FUS RRM. Using a pulse scheme described previously,[17] NOESY data sets were recorded on an 800 MHz spectrometer at 25 °C to measure intermolecular contacts between aromatic protons coupled to ^{13}C in the CAPRIN1 scaffold and amides in FUS RRM client molecules. The ^{13}C carrier was positioned at 125 ppm and aromatic protons were selectively excited by applying 0.64 ms on-resonance ^{13}C REBURP pulses during INEPT and reverse-INEPT periods. NOESY data sets were recorded at 25 °C using an HSQC readout with an interscan delay of 1.5 s, 188 scans/FID, a NOE mixing time of 250 ms, and ^{15}N $t_{1,max}$ = 50 ms, for a total acquisition time of ∼24 h.

https://doi.org/10.1021/jacs.5c10918
J. Am. Chem. Soc. 2025, 147, 33071−33085

The FUS RRM interaction sites in CAPRIN1 were identified via a complementary NOESY experiment performed on a mixed solution sample containing 0.7 mM $^{1}H,^{13}C,^{14}N$-labeled FUS RRM and 0.5 mM $^{2}H,^{12}C,^{15}N$ CAPRIN1. In this case, NOEs between all protons attached to ^{13}C in the FUS RRM client and protons coupled to ^{15}N in the CAPRIN1 scaffold were measured. The ^{13}C carrier was positioned at 67.5 ppm and all protons were uniformly excited by applying 0.4 ms adiabatic pulses during INEPT and reverse-INEPT transfers. A NOESY data set was recorded on a 1 GHz spectrometer at 25 °C using an HSQC readout with an interscan delay of 1.5 s, 224 scans/FID, NOE mixing time of 250 ms, and ^{15}N $t_{1,max}$ = 50 ms, for a total acquisition time of ∼24 h 30 min.

2D [$^{1}H,^{13}C$]-HSQCs for Determining CAPRIN1 and pYCAPRIN1 Condensed Phase Concentrations and Partition Coefficients of FUS RRM in Phase-Separated CAPRIN1 and pYCAPRIN1 Solutions (Figure 5; 600 MHz). $^{2}H,^{15}N,^{13}C$-ILV FUS RRM, and unlabeled CAPRIN1 and pYCAPRIN1 were buffer exchanged into 20 mM HEPES pH 7, 0.5 mM EDTA, 200 mM NaCl buffer and concentrated at 40 °C using 3 kDa molecular weight cutoff amicon spin filters. Note that at this [NaCl] and temperature combination of 200 mM and 40 °C, respectively, both CAPRIN1 and pYCAPRIN1 do not phase separate at concentrations up to several millimolar. However, when the temperature is reduced, phase separation is induced. In this regard, FUS RRM was added to the CAPRIN1 and pYCAPRIN1 nonphase-separated solutions to a final concentration of 40 μM and the mixtures were kept in a ∼42 °C water bath for 30 min. The falcon tubes containing the FUS RRM:(pY)CAPRIN1 solutions were placed on ice for 1 h to induce phase separation. The droplets were fused through centrifugation at 4,000 g for 10 min. The falcon tubes were placed back on ice, and 15 μL (5 μL) of dilute (condensed) phase was carefully pipetted out and placed into Eppendorf tubes. An additional 15 μL (5 μL) was removed for duplicate measurements to estimate errors. Samples were prepared by addition of 127.5 μL of 8 M urea buffer, 7.5 μL D_2O (dilute phase, net volume 150 μL) with an additional 10 μL of buffer added for the condensed phase, so that the concentrations of urea are the same in both cases (6.8 M). The net dilutions of the condensed and dilute phases were, thus, 30 and 10-fold, respectively. The final pH of the urea-treated solutions was ∼ 8.

The (pY)CAPRIN1 concentrations in the 30-fold diluted condensed phase samples were measured using 2D [$^{1}H,^{13}C$]-HSQCs. Condensed phase concentrations were determined by comparing the volumes of (pY)CAPRIN1 natural abundance alanine and threonine signals to the volumes quantified in reference (pY)CAPRIN1 solutions of known concentrations, taking into account the differences in the number of scans and dilution factors. Similarly, the partition coefficients (K_p) of FUS RRM in CAPRIN1 and pYCAPRIN1 phase-separated solutions were determined by comparing volumes of Ile peaks in 2D [$^{1}H,^{13}C$]-HSQCs recorded on condensed vs. dilute phase samples, taking into account the differences in the number of scans and dilution factors. Note that FUS RRM is fully unfolded at 6.8 M urea and all unfolded isoleucine methyl group signals are largely degenerate giving rise to a set of overlapping peaks, the total volume of which is determined using a sum-overbox approach.

RESULTS

Hydrodynamic Properties of the Folded FUS RRM Client in the Condensed Phase at 25 °C. Our initial studies of client:scaffold interactions were focused on a metastable variant of the ALS protein superoxide dismutase 1 (SOD1) that *in cell* partitions into stress granules containing CAPRIN1 as one of the scaffold proteins.[35] In a SOD1:CAPRIN1 model system that we have studied previously the folding/unfolding equilibrium of SOD1 is shifted significantly to the unfolded state (∼70% at 25 °C), leading to the aggregation of both SOD1 and CAPRIN1 over time.[5] Studies at temperatures higher than 25 °C were, therefore, not possible, and we were not able to observe $^{1}H-^{15}N$ correlation spectra of folded SOD1 under these conditions. Similarly, amide correlation spectra of folded FUS RRM in CAPRIN1 condensates were of very poor quality when recorded at 25 °C[20] (see below). In this case we wondered whether the absence of peaks reflected the high viscosity of the condensed phase and/or perhaps, the relatively low concentrations of FUS RRM that could partition inside. In our previous study of SOD1 in CAPRIN1 condensates it was established that NMR experiments were not concentration limited; rather, the high condensate viscosity precluded detection of amide signals.[5] To investigate this further in the context of FUS RRM, we first measured the translational diffusion of the CAPRIN1 scaffold in both condensed and dilute phases, to characterize the local viscosity that would be "experienced" by the folded client in each environment. At 25 °C, the concentrations of CAPRIN1 in the dilute and condensed phases are 29 and 321 mg/mL, respectively, while the water content is 973 and 810 mg/mL, suggesting significantly higher solution viscosity in the condensed phase.[20] Focusing on the CAPRIN1 methionine methyl groups which produce intense signals in 1D ^{13}C-edited spectra even at natural abundance, we recorded triple-quantum and single-quantum diffusion experiments on the condensed and dilute phase samples, respectively (Figure 1B, left). Note that the effective diffusion constant in the triple-quantum experiment is scaled by a factor of 9 relative to the corresponding single-quantum experiment, extending the effective molecular weight of particles that can be studied by approximately 3 orders of magnitude.[25] The triple-quantum approach is thus well-suited for measurements in the highly viscous condensed phase. Our experiments establish that the diffusion of scaffold molecules is slowed by approximately 20-fold in the condensed vs. dilute phase at 25 °C (Figure 1B, right).

To obtain a direct understanding of the hydrodynamic properties of the folded FUS RRM client in the FUS RRM:CAPRIN1 condensed phase, we recorded methyl-TROSY delayed-decoupling NMR experiments[21] on a sample of highly deuterated FUS where only methyl groups of Ile (δ1), Leu(δ1,δ2), and Val(γ1, γ2) are NMR observable ($^{13}CH_3$) and where the prochiral methyls of Leu and Val are labeled as $^{13}CH_3$, $^{12}CD_3$ in a nonstereospecific manner[36] (Figure 1C). In order to ensure that signals from the CAPRIN1 L,V methyl groups do not obscure those from FUS RRM we have mutated Leu 621 and Val 610 in the scaffold to Ala, as described previously,[21] and in Methods (there are no Ile residues in CAPRIN1). It thus becomes possible to record methyl-relaxation experiments such as those based on triple-quantum relaxation violated coherence transfer (Figure 1D) from which the product $S^2_{Axis}\tau_{c,eff}$ is obtained.[37] In the simplest model S^2_{Axis} is related to the amplitude of motion of the methyl 3-fold axis and $\tau_{c,eff}$ is a methyl group specific effective correlation time for the overall tumbling of the methyl symmetry axis (Figure 1D, inset). Shown in Figure 1D are profiles from measurements for methyl groups of the folded FUS RRM domain in the condensed phase (*purple*) and in buffer (*yellow*), recorded at 25 and 5 °C, respectively. Neglecting the slight changes in S^2_{Axis} values with temperature,[38] $S^2_{Axis}\tau_{c,eff}$ measured at 5 °C can be scaled to 25 °C by multiplying by 0.55 which takes into account the viscosity change of water with temperature as well as the absolute temperature difference between the measurements. A histogram of the scaled $S^2_{Axis}\tau_{c,eff}$ values is shown in Figure 1E for FUS RRM in the condensed phase and in buffer, as well as for

https://doi.org/10.1021/jacs.5c10918
J. Am. Chem. Soc. 2025, 147, 33071−33085

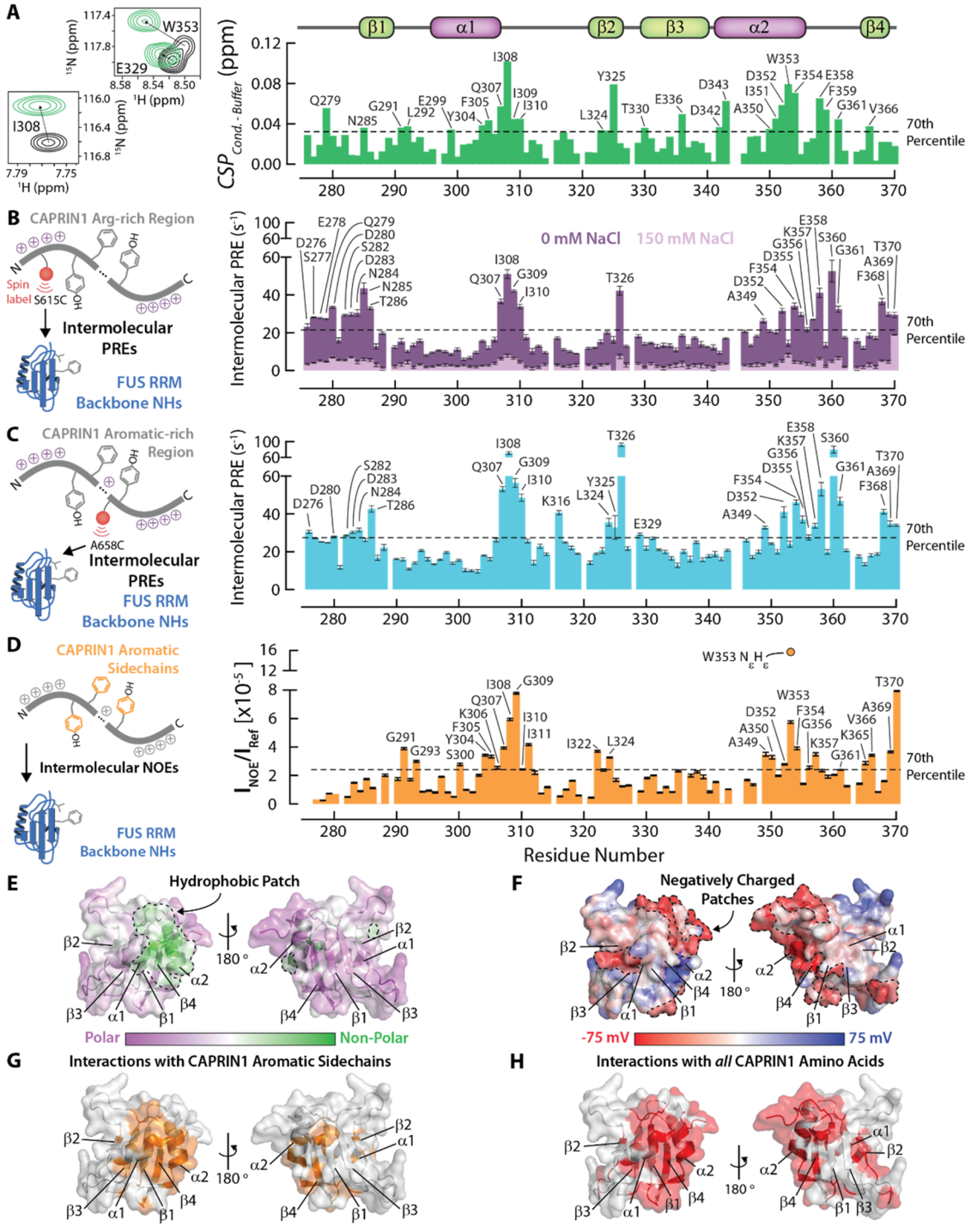

Figure 3. CAPRIN1 interaction sites in FUS RRM. (A) CAPRIN1 interaction sites in FUS RRM as probed through chemical shift perturbations (CSPs) of FUS RRM amide resonances in [^{1}H,^{15}N]-HSQC spectra (*left*) recorded in the condensed phase (*green*) vs. buffer (*black*). Residue-specific chemical shift perturbations (*green bars*) of FUS RRM, calculated as $n\sqrt{(\delta_H{}^2 + (0.2*\delta_N)^2)}$, where δ_H and δ_N are the ^{1}H and ^{15}N chemical shift differences for a given residue between condensed phase and buffer, respectively. Residues with CSPs in the 70th percentile and above are annotated. The FUS RRM secondary structure elements are schematized above. The bulk concentration of NaCl in the phase-separated solution and in buffer is 200 mM. (B−C) CAPRIN1 interaction sites within FUS RRM, probed in buffer solutions lacking NaCl, unless otherwise indicated. Probing FUS RRM interactions with (**B**) N-terminal arginine-rich and (C) central aromatic regions in CAPRIN1, using intermolecular PRE experiments wherein a DOTA cage coordinated with either gadolinium (paramagnetic) or lutetium (diamagnetic) was conjugated onto position S615C (B) or A658C (**C**) of CAPRIN1. Intermolecular PREs originating from the CAPRIN1 N-terminal arginine-rich region (S615C) were measured in mixed solution samples containing 0 mM (*purple bars*) and 150 mM (*pink bars*) NaCl. Residues with intermolecular PREs in the 70th percentile and above are annotated. (D) Interaction sites of CAPRIN1 aromatic residues in FUS RRM, as probed through intermolecular NOE experiments recorded in a mixed solution sample in the absence of NaCl, quantifying magnetization transfer from aromatic protons attached to ^{13}C in CAPRIN1 to protons bonded to ^{15}N in FUS RRM (Methods). Residues with intermolecular NOEs in the 70th percentile and above are annotated. (E)−(F) Visualization of hydrophobic (E) and charged (F) patches on the surface of FUS RRM (AlphaFold predicted structure). In

https://doi.org/10.1021/jacs.5c10918
J. Am. Chem. Soc. 2025, 147, 33071−33085

Figure 3. continued

(E), the ratio of nonpolar to polar solvent accessible surface area (NPP) is mapped onto FUS RRM, with low (high) NPP ratio shown in purple (green), while in (F) the negative (positive) charged surfaces are color-coded in red (blue).[49] (G) All residues significantly interacting with CAPRIN1 aromatic side chains (in the 70th percentile and above in panel (D)) are mapped (*orange*) onto the AlphaFold predicted FUS RRM structure. (H) All residues significantly interacting with *any* CAPRIN1 amino acid (residues in the 70th percentile and above in panels (B−D) are mapped onto the AlphaFold predicted FUS RRM structure.

the nucleosome core particle (NCP; only methyl groups within the core are included), for comparison. Averages values of 92.9 ± 22.6 and 71.2 ± 21.4 are obtained for FUS RRM in the CAPRIN1 condensate and for the NCP in buffer, respectively, (error indicates 1 standard deviation) indicating similar overall tumbling rates under the measurement conditions, after scaling all data to a temperature of 25 °C. Assuming that maximum values of $S^2_{Axis}\tau_{c,eff}$ correspond to the case where $S^2_{Axis} = 1$, $\tau_{c,eff}$ of 132.9 and 118.9 ns are calculated for FUS RRM and the NCP, respectively, that suggest that folded FUS RRM in the CAPRIN1 condensate at 25 °C tumbles with a similar effective correlation time as that of a 210 kDa particle in buffer.

Exploiting the Steep Temperature Dependence of CAPRIN1 Condensate Viscosity for Recording ^{1}H−^{15}N Correlation Spectra of Folded FUS RRM. We wondered whether high quality amide spectra of the folded FUS RRM domain could be recorded in the CAPRIN1 condensed phase, similar to methyl-TROSY data sets, by elevating the temperature. Notably, raising the temperature from 25 to 40 °C increased the CAPRIN1 diffusion constant in the condensed phase by 7-fold (Figure 2A). When compared to the diffusion of CAPRIN1 in the dilute phase at 25 °C (Figure 1B) the diffusion rate of CAPRIN1 in the condensate at 40 °C is only 3-fold reduced, suggesting that significant improvements to the spectral quality of [^{1}H−^{15}N]-HSQC data sets recorded in condensates should be feasible by increasing the temperature by 10−15 °C. This is illustrated in Figure 2B, where a superposition of data sets recorded at 25 °C (*purple*) and 40 °C (*green*) is shown. The peaks observed in the lower temperature spectrum derive from the unfolded FUS RRM state, as is clear from the narrow distribution of amide proton chemical shifts centered at approximately 8 ppm, as well as from the CAPRIN1 scaffold whose effective concentration in ^{15}N is approximately 90 μM. Note that the fractional population of folded FUS RRM at 25 °C is approximately 70% with an absolute concentration of 340 μM[20] (inset), yet tumbling is too slow to observe the amide correlations. In contrast, correlations at 40 °C extend to 9.5 ppm, with the downfield peaks originating from residues in secondary structure elements of folded FUS RRM. Amide correlations derived from the folded conformer are, thus, observed, even though the folded state is ∼40% populated and the concentration reduced to 200 μM,[20] both close to a factor of 2 less than at 25 °C. Figure 2C plots backbone ^{15}N transverse relaxation rates (R_2) for FUS RRM as a function of residue in the buffer and condensed phase samples, 40 °C, with the data displayed as a linear correlation plot in Figure 2D. From fits of ^{15}N R_1, R_2, and ^{15}N{^{1}H} steady state NOE values an effective correlation time, $\tau_{c,eff}$, of 4.6 ns for FUS RRM dissolved in buffer is obtained, assuming isotropic tumbling. This value is then used along with the slope of the correlation plot of Figure 2D to estimate a value of 27.1 ns for the assumed isotropic tumbling of the folded FUS RRM domain in the CAPRIN1 condensate, 40 °C ($\frac{R_{2,cond}}{R_{2,buff}} \cdot \tau_{c,eff}^{buff}$.). Using the empirical relationship[39] $\tau_{c,eff}$ (ns) ≈ 0.43 × MW (kDa), an apparent molecular weight of ∼60 kDa is computed. Collectively, these findings demonstrate that if the client-scaffold phase-separated system remains stable at 40 °C, close to physiological temperature, the tumbling of small folded proteins in the condensed phase can be brought into a regime that supports high-resolution ^{1}H−^{15}N correlation spectroscopy. In the case of the FUS RRM:CAPRIN1 system, we previously showed that dissolution in the condensed phase prevents FUS RRM aggregation due to "protective" interactions with CAPRIN1.[20] Working at 40 °C is, thus, an excellent option for this system.

Mapping CAPRIN1 Scaffold Interaction Sites within the FUS RRM Client. Having identified a temperature where high-quality amide correlation spectra of a folded client can be obtained in the condensed phase, we next sought to map, at residue-resolution, the scaffold interactions that drive client partitioning into the condensate from the perspective of its folded state. To this end, we first compared [^{1}H,^{15}N]-TROSY-HSQC spectra of FUS RRM in buffer and in the CAPRIN1 condensed phase (Figure S2A, black vs green). Notably, the condensed phase spectrum contains additional peaks arising from a significant population of unfolded FUS RRM molecules and from the highly concentrated CAPRIN1 scaffold (∼90 μM of 0.3% ^{15}N natural abundance CAPRIN1) in this environment, as discussed above. We focused on changes in the positions of peaks derived from the folded state of FUS RRM in buffer vs. CAPRIN1 condensed phase (Figure S2A, black vs green, annotated residues), which reflect changes in the local environment of FUS RRM arising from interactions with CAPRIN1. Slight, but quantifiable, differences in peak positions (chemical shift perturbations, CSPs) are observed (Figure S2A). Residues with the largest CSPs, *i.e.*, the top 30th percentile, map to several regions in FUS RRM including β2, the residues surrounding β1, and the C-terminal ends of the α1 and α2 helices (Figure 3A, annotated residues).

To obtain further insight into the nature of the heterotypic FUS RRM:CAPRIN1interactions we carried out several experiments on mixed samples (at concentrations of several hundreds of μM of each protein component). Studies under these conditions benefit from high sensitivity, as sample viscosities are much reduced relative to the condensed phase (demixed), so that amide-based experiments more complex than simple HSQCs can be recorded in a rapid and quantitative manner. This is particularly germane when results from different experiments are to be compared, necessitating the use of consistent sample concentrations which can be difficult to control in the condensed phase environment. In the first set of experiments, we introduced PRE-based probes at distinct CAPRIN1 regions with unique amino acid compositions and examined their interaction sites on the FUS RRM domain. To this end, we produced cysteine mutations at either S615 or A658 (one at a time) into an otherwise cysteine-less CAPRIN1 construct, and conjugated a 1,4,7,10-tetraazacyclododecane-1,4,7,10-tetraacetic acid (DOTA) cage loaded with either gadolinium (Gd^{3+}, paramagnetic) or lutetium (Lu^{3+},

https://doi.org/10.1021/jacs.5c10918
J. Am. Chem. Soc. 2025, 147, 33071−33085

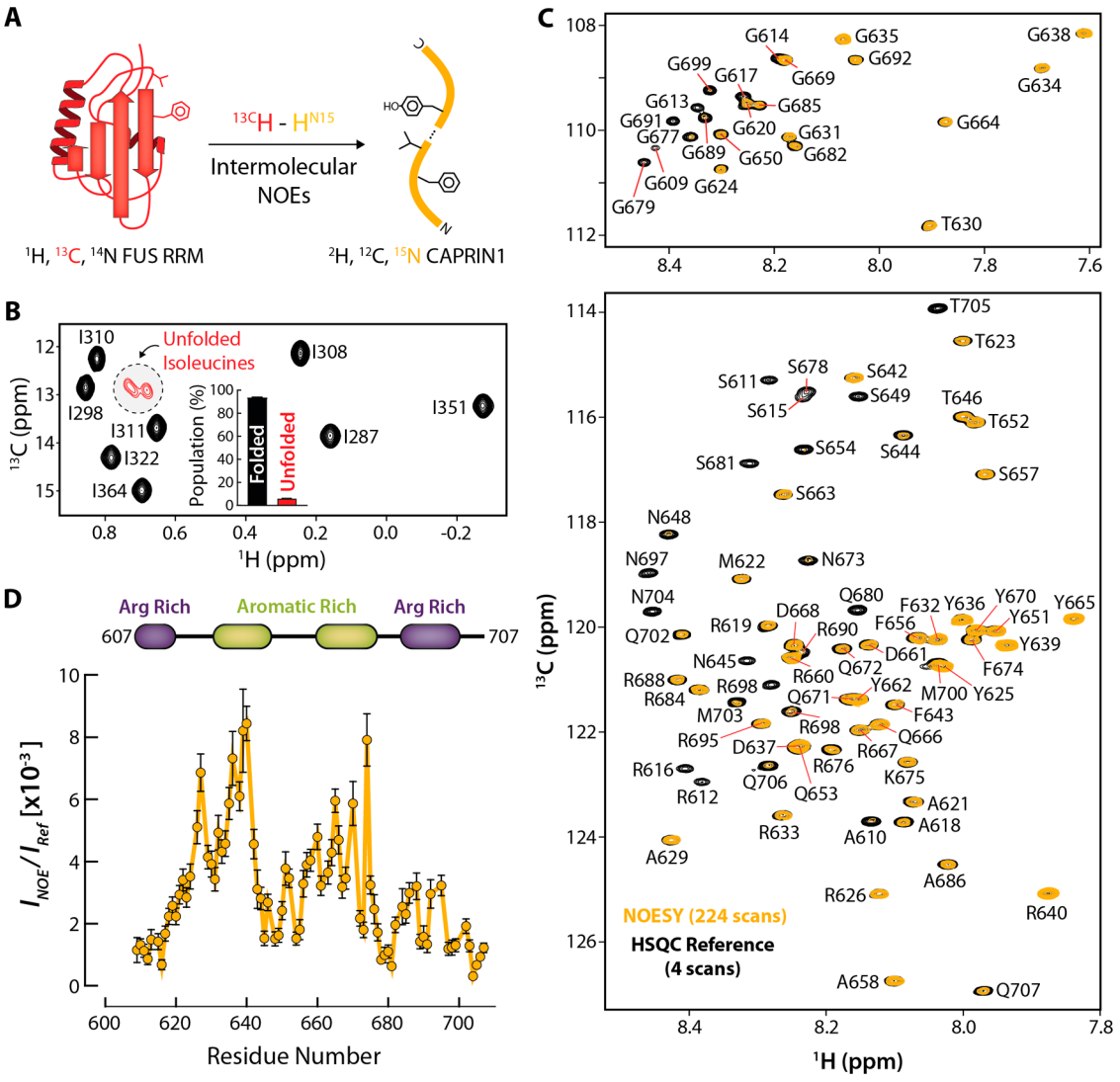

Figure 4. FUS RRM folded conformer interaction sites in CAPRIN1. (A) Schematic of the intermolecular NOE experiment quantifying magnetization transfer from protons attached to ^{13}C in FUS RRM (*red*) to protons bonded to ^{15}N in CAPRIN1 (*yellow*). (B) Methyl-TROSY spectrum of 0.7 mM ^{1}H, ^{13}C, ^{14}N FUS RRM in the presence of 0.5 mM ^{2}H, ^{12}C, ^{15}N CAPRIN1 in pH 6 buffer recorded at 25 °C, indicating that FUS RRM is primarily folded (94%) under these conditions (*panel inset*). Peak volumes from Ile residues derived from folded (*black*) and unfolded (*red*) FUS RRM were used to compute the populations, with the total volume of the overlapping unfolded resonances determined using a sum-overbox approach. (C) Zoomed-in expansions from the intermolecular NOE experiment illustrated schematically in A, and recorded using the mixed solution sample described in B with a mixing time of 250 ms at 1 GHz, 25 °C. The NOESY spectrum (*yellow*) is superimposed onto the corresponding regions from a [^{1}H,^{15}N]-HSQC spectrum (*black*). Note that the NOESY spectrum is recorded with 56-times the scans of the HSQC. (D) Intermolecular NOE profile (*yellow symbols*) after normalizing NOE peak intensities to the intensities of the corresponding amide correlations in an HSQC data set and accounting for the differences in the numbers of scans in the two experiments. Regions of CAPRIN1 enriched in arginine (*purple*) and aromatic (*green*) residues are annotated above the profile.

diamagnetic) via a maleimide linkage. Uniformly ^{15}N,^{13}C-labeled FUS RRM was mixed with equimolar amounts of either paramagnetic or diamagnetic ^{14}N-CAPRIN1 and intermolecular interactions were read out through [^{1}H,^{15}N]-HSQC spectra. As Gd^{3+} possesses seven unpaired f-electrons ($S = 7/2$), it generates a strong magnetic field that induces distance-dependent attenuation of proximal protons in FUS RRM, whereas Lu^{3+} ($S = 0$) does not. Consequently, peaks in the Gd-DOTA–tagged CAPRIN1 spectrum are attenuated relative to those in the Lu-DOTA spectrum. This PRE effect provides a direct measure of intermolecular interactions, which can be quantified through amide proton relaxation rates (Figure S2B).

Results from experiments using CAPRIN1 spin-labeled in the N-terminal arginine-rich region (S615C) are in agreement with FUS RRM interaction sites identified through CSPs (Figure 3B, purple bars vs 3A, green bars). Notably, increasing the sample salt concentration markedly attenuated intermolecular interactions across the entire FUS RRM sequence (Figure 3B, pink bars vs purple bars, Figure S2C), indicating a dominant contribution from electrostatic interactions. To determine whether additional FUS RRM interaction sites exist within CAPRIN1, we recorded spectra with the spin-label introduced between the two CAPRIN1 aromatic-rich regions (A658C, Figure 3C). The resulting intermolecular PRE profile closely resembles that observed with the N-terminal arginine-rich probe (Figure 3C vs 3B). However, the magnitudes of the

https://doi.org/10.1021/jacs.5c10918
J. Am. Chem. Soc. 2025, 147, 33071−33085

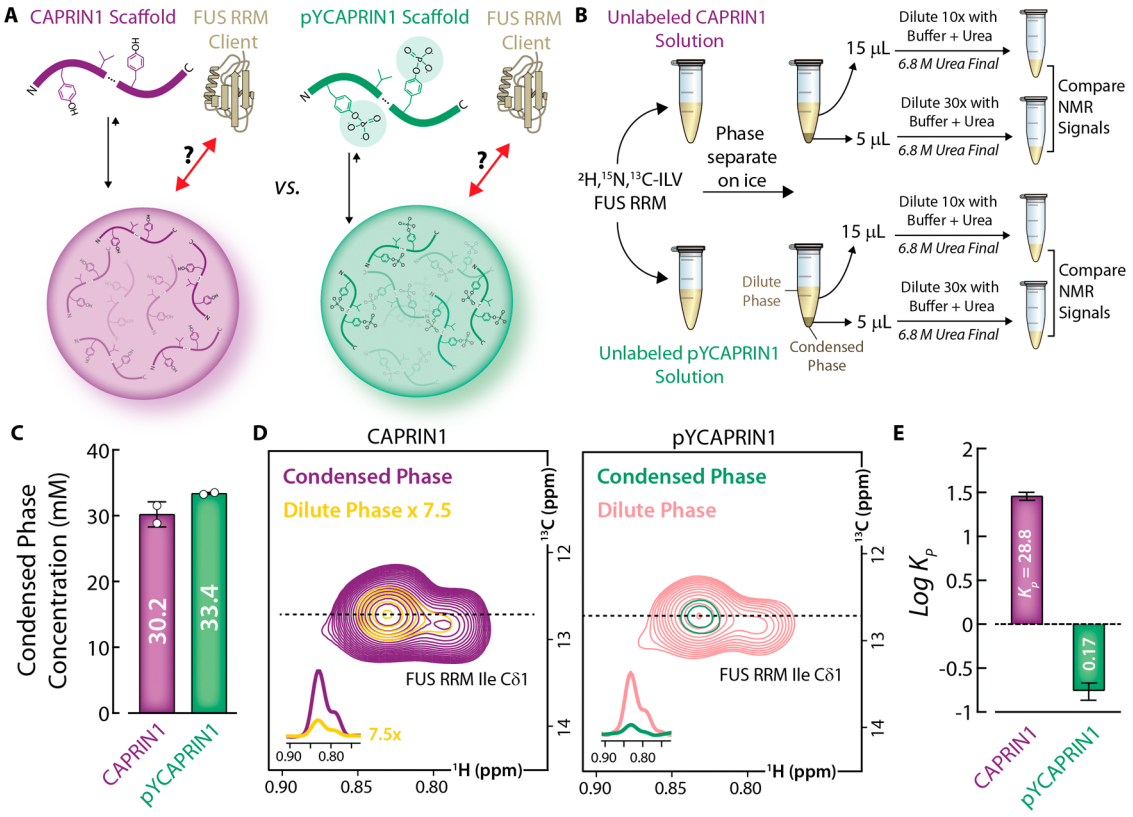

Figure 5. Tyrosine phosphorylation of CAPRIN1 reduces partitioning of FUS RRM into the condensed phase. (A) Schematic highlighting partitioning of FUS RRM into CAPRIN1 (left) and phosphorylated CAPRIN1 (pYCAPRIN1, right) condensates (*red arrows*). (B) Diagram illustrating how FUS RRM partition coefficients were measured in phase-separated solutions of CAPRIN1 (*top*) and pYCAPRIN1 (*bottom*). Experiments were performed in duplicates for error estimation. Details are provided in Methods. (C) Concentrations of CAPRIN1 (*purple*) and pYCAPRIN1 (*green*) in the condensed phase, as determined through comparison of CAPRIN1 (pYCAPRIN1) aliphatic ^{1}H signals with those in spectra recorded on reference samples of known CAPRIN1 (pYCAPRIN1) concentrations. (D) Select regions of [^{1}H, ^{13}C]-HSQCs of the dilute and condensed phases of CAPRIN1 and pYCAPRIN1 phase-separated solutions after dilution with urea (as indicated in B), focusing on the FUS RRM isoleucine Cδ1 methyl signals. Differences in dilution factors and number of scans are accounted for so that differences in peak intensities purely reflect differences in FUS RRM concentration in the two phases. The FUS RRM signals in the CAPRIN1 dilute phase were scaled-up by 7.5 fold for the purpose of visualization. Slices through the ^{1}H dimension at the positions of the black dashed lines are shown in the panel insets. (E) Log partitioning coefficients, K_p, of FUS RRM into CAPRIN1 (*purple*) and pYCAPRIN1 (*green*) condensed phases. Values of K_p are indicated inside each of the rectangles in the figure.

PREs are substantially greater when the label is positioned between the CAPRIN1 aromatic-rich regions, suggesting a significant contribution from interactions involving aromatic residues. In order to selectively evaluate the importance of aromatic residues to FUS RRM − CAPRIN1 contacts we performed an experiment designed to specifically probe interactions mediated by aromatic side chains. To this end, we recorded an intermolecular NOE spectrum using a sample containing ^{1}H,^{13}C,^{14}N CAPRIN1 and ^{2}H,^{15}N FUS RRM. Magnetization transfer from ^{13}C-bound aromatic protons in CAPRIN1 to FUS RRM amide protons (Figure 3D, left) was detected in a 2D [^{1}H−^{15}N] correlation data set (Figure S2D), as previously described,[17] with the labeling scheme used ensuring that NOEs only derive from intermolecular transfer. Notably, interactions with the N-terminal, negatively charged region of FUS RRM (~D276-T286) are weak, whereas other interaction sites noted in the PRE-based experiments were stronger (Figure 3D, right). Of interest, the interactions with CAPRIN1 aromatic residues primarily localize to a hydrophobic patch on the surface of FUS RRM (Figure 3G, orange vs Figure 3E, green), while the remaining interactions largely localize to negatively charged regions on the FUS RRM surface (Figure 3H, red vs Figure 3F, red).

Mapping FUS RRM Client Interaction Sites within the CAPRIN1 Scaffold. To establish FUS RRM:CAPRIN1 interactions, this time from the side of CAPRIN1, we prepared a mixed solution sample consisting of 0.7 mM ^{1}H,^{13}C,^{14}N FUS RRM and 0.5 mM ^{2}H,^{15}N CAPRIN1 and performed NOE experiments using a magnetization transfer scheme illustrated in Figure 4A. Here magnetization is transferred from all ^{13}C-bound protons of FUS RRM to amide protons on CAPRIN1. Our choice of a mixed, rather than condensed phase sample was based on several factors. First, a condensed phase sample would require prohibitively large amounts of (expensive) ^{2}H,^{12}C CAPRIN1 to suppress intermolecular CAPRIN1:CAPRIN1 NOEs that potentially could arise from the otherwise high concentrations of the ^{1}H,^{12}C CAPRIN1 scaffold (~30 mM) and the 1% natural abundance ^{13}C isotopomer population. Moreover, under these conditions, a significant population of FUS RRM would be unfolded[20] (Figure 2B) leading to NOEs from both folded and unfolded client molecules that cannot be separated using the sensitive 2D scheme of Figure 4A. In contrast, under the dilute protein conditions used here (0.5 mM CAPRIN1), the unfolding equilibrium is heavily skewed toward the folded state with a

https://doi.org/10.1021/jacs.5c10918
J. Am. Chem. Soc. 2025, 147, 33071−33085

fractional population of 94% for the folded conformer (Figure 4B), and therefore, the NOEs observed are predominantly those connecting folded FUS RRM with CAPRIN1.

Figure 4C shows a superposition of the NOESY spectrum (*orange*) recorded with a mixing time of 250 ms with the corresponding regions from a reference [^{1}H−^{15}N]-HSQC data set (*black*), both acquired at 25 °C. The NOE intensities are weak, as is clear from the relative numbers of scans accumulated in each experiment, consistent with the transient, solvent-like nature of the interactions. Intensity ratios of NOE vs. HSQC crosspeaks are shown in Figure 4D, where NOE intensities were first normalized by taking into account the number of scans recorded for each data set. Notably, the most intense NOEs connect FUS RRM with the aromatic-rich central region of CAPRIN1 (see domain architecture above), while the arginine rich moieties on either ends of the CAPRIN1 construct form more distal, weaker contacts. Collectively, the results highlighted in Figures 3 and 4D indicate that FUS RRM recruitment into the CAPRIN1 condensate is driven by electrostatic interactions between negatively charged FUS RRM regions and positively charged segments of CAPRIN1, along with strong contributions from interactions involving CAPRIN1 aromatic residues.

Tyrosine Phosphorylation of CAPRIN1 Reduces Partitioning of FUS RRM into the Condensed Phase. Having identified key interactions that drive partitioning of FUS RRM into CAPRIN1 condensates, we next asked how chemical modifications to the scaffold—such as post-translational modifications—might modulate client−scaffold interactions and, in turn, affect client partitioning. To this end, we phosphorylated several tyrosine residues of CAPRIN1, incorporating an average of five phosphate groups per CAPRIN1 chain (Figure S3). This modification caused the net charge of CAPRIN1 at pH 7, the pH used to prepare the phase-separated sample, to shift from +13*e* to +3*e* (Figure 5A), where *e* is the elementary charge. This modification is expected to alter not only the electrostatic interactions with negatively charged (−5*e*) FUS RRM chains, but also the contacts involving CAPRIN1's aromatic residues. Solutions of unmodified, unlabeled CAPRIN1 and tyrosine-phosphorylated, unlabeled CAPRIN1 (pYCAPRIN1) were prepared and separately mixed with substoichiometric amounts (<15 fold) of ^{2}H,^{15}N,^{13}C-ILV FUS RRM client and allowed to phase separate on ice (Figure 5B). Aliquots from both the dilute and condensed phases of FUS RRM:(pY)CAPRIN1 mixtures were collected and diluted with urea (pH 8) to generate homogeneous solutions for NMR analysis (Figure 5B), with 2D [^{1}H,^{13}C]-HSQCs recorded for samples originating from both the dilute and condensed phases of FUS RRM:(pY)CAPRIN1. Volumes of spectral peaks unique to (pY)-CAPRIN1 and FUS RRM were quantified to determine the relative concentrations of the two proteins in condensed vs. dilute phases. Further, comparison of these peak volumes with those quantified from reference samples of known concentration led to estimates of 30.2 ± 1.9 and 33.4 ± 0.2 mM for CAPRIN1 and pYCAPRIN1, respectively, in their condensed phases (Figure 5C). Under these conditions, a greater than 2 orders of magnitude increase in the partitioning of FUS RRM into CAPRIN1 vs. pYCAPRIN1 condensed phases is observed (Figure 5D,E), with FUS RRM partitioning coefficients ($K_p = \frac{[FUS]_{cond}}{[FUS]_{dilute}}$) of 28.8 ± 2.98 and 0.17 ± 0.04. These results indicate that phosphorylation of CAPRIN1 tyrosine side chains modulates interactions with FUS RRM that, in turn, diminishes the preferential solvation and recruitment of FUS RRM into the condensed phase. While these experiments, in principle, do not discriminate between folded and unfolded FUS in each of the condensed and dilute phases, they were carried out at 0 °C where the unfolded state is only negligibly populated (3.2 and 0.6%, respectively). Therefore, the K_p values obtained in this manner largely report on the partitioning of the folded FUS domain between the two phases.

DISCUSSION

Biomolecular condensates are dynamic assemblies with distinct molecular compositions that can change in response to cellular stimuli, concentrating anywhere from a few to several hundreds of different biomolecules.[1] The fidelity of the cellular processes they mediate depends on the precise inclusion of specific components and the exclusion of others. Therefore, developing a general framework to understand condensate composition is central to elucidating how cells execute their functions. Recent efforts toward this goal have primarily focused on the contributions of intrinsically disordered protein regions (IDRs) to the selective partitioning of clients into condensates. For example, the Sabari group conducted proteomic analyses of proteins that partition into or are excluded from condensates scaffolded by the MED1 IDR, both in nuclear extracts and intact cells.[40,41] Their analyses revealed that ∼67% of partitioned clients in nuclear extracts contain IDRs of 30 or more residues, and that the sequence features of these regions differentiate between highly partitioned vs. excluded proteins. While these findings provide compelling evidence that selective partitioning is, in part, encoded in the sequence of disordered regions, they also raise important questions about the physicochemical features governing the partitioning of the remaining ∼33% of proteins that lack substantial IDRs.

Machine-learning, particularly large language models trained on data sets of protein sequences with experimentally annotated condensate localizations, such as ProtGPS,[42] have also advanced our ability to predict client partitioning with high accuracy. However, these models focus on disordered protein sequences and have been validated on *de novo*-designed IDR sequences to minimize confounding effects from folding.[42] Thus, they offer limited insights for folded clients lacking substantial IDRs, whose sequence information alone may not reflect features relevant to condensate partitioning, as many residues in folded domains remain buried and are unlikely to mediate interactions.[41] Thus, new approaches are needed to understand the partitioning of folded clients, especially those that assess client-scaffold interactions from a structural perspective, focusing on the properties of solvent-exposed surfaces that may mediate interactions with condensate scaffolds.

NMR spectroscopy is well poised to provide detailed, atomistic insights into the structure, dynamics and interactions of both scaffold and client components. To date, most efforts have focused on disordered proteins,[10−17,43,44] due to their favorable segmental backbone dynamics, which help offset the increased viscosity of the condensed phase. This enables the acquisition of high-quality amide correlation spectra, allowing site-specific interactions to be mapped across the entire protein sequence. Methyl-TROSY-based experiments,[45] optimized for the challenges posed by the highly concentrated and viscous condensed phase environment, now enable characterization of

https://doi.org/10.1021/jacs.5c10918
J. Am. Chem. Soc. 2025, 147, 33071−33085

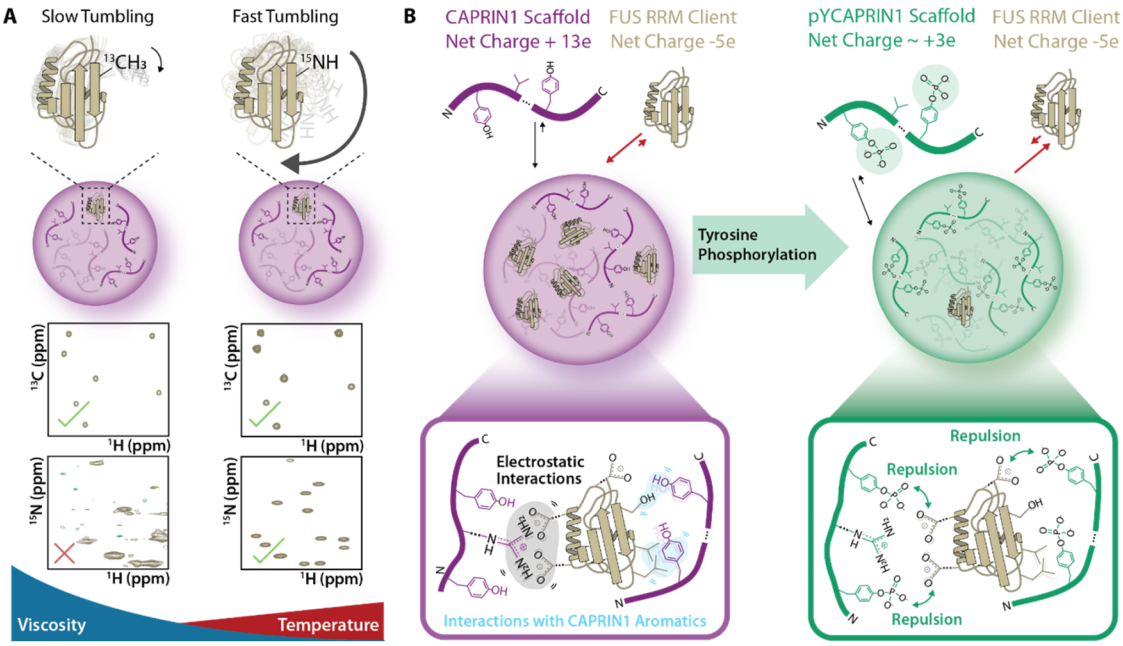

Figure 6. Overview of NMR methods for probing client-scaffold interactions across different experimental regimes and how such interactions regulate client partitioning into condensates. (A) Schematic illustrating how the steep temperature-dependence of condensate viscosity can be exploited in studies of client-scaffold interactions. At low temperatures, where condensate viscosity is high and folded client proteins tumble slowly, client NMR signals are principally observed through methyl-TROSY approaches. At higher temperatures, the solution viscosity is significantly reduced, enabling detection of fast tumbling folded clients through amide-correlation spectroscopy. (B) Electrostatic interactions (*black shaded region, left*) between the positively charged (+13e) CAPRIN1 scaffold and the negatively charged (−5e) FUS RRM client as well as interactions involving CAPRIN1 aromatic residues (*blue shaded region, left*) drive the enrichment of FUS RRM into CAPRIN1 condensates. Phosphorylation of CAPRIN1 Tyr residues reduces the net charge to ~ +3e, weakening electrostatic interactions, and decreasing the strength of contacts involving CAPRIN1 Tyr (*green arrows, right*), resulting in a dramatic reduction of FUS RRM partitioning into pYCAPRIN1 condensates.

molecular interactions involving methyl-bearing amino acids in folded client proteins.[21] However, complementary experiments that provide residue-specific readouts across the full-sequence of a folded protein would be advantageous for obtaining a comprehensive understanding of the client-scaffold interactions driving client partitioning.

In this regard, for the folded FUS RRM client:CAPRIN1 scaffold system studied here, we demonstrate that the condensate viscosity exhibits a steep temperature dependence, with the translational diffusion rate of the CAPRIN1 scaffold increasing 7-fold between 25 and 40 °C - a change comparable to the viscosity decrease observed for 70% (v/v) glycerol over this temperature interval.[46] Notably, at 40 °C, the rotational correlation time of the folded FUS RRM client in the condensed phase is approximately 27 ns, enabling the acquisition of high quality $^{15}N-^{1}H$ spectra under these conditions (Figure 6A).

Using a combination of intermolecular NOEs and PREs recorded in mixed solutions, and chemical shift perturbation mapping based on experiments performed in the condensed phase, all with a [$^{1}H-^{15}N$]-HSQC readout, we identified multiple interaction surfaces in FUS RRM that contact the CAPRIN1 scaffold. These include a negatively charged patch in the N-terminal region spanning D276-T286, as well as two major regions near the C-terminal ends of the α1 and α2 helices, roughly encompassing residues ~Q307-I310 and ~A350-G361, respectively. Additional localized interaction sites were observed at ~L324-T326 and ~F368-T370, indicating that client-scaffold interactions are mediated by a distributed set of contact points across the FUS RRM surface, consistent with a high valence mode of interaction rather than a single interface (Figure 6B, left). Unlike a typical aqueous buffer, where water is the primary solvent, the CAPRIN1 proteinaceous environment contributes a complex and diverse set of solvent interactions. Indeed, PRE measurements show that intermolecular contacts are strongest when spin labels are introduced into the aromatic-rich segments of CAPRIN1 and are attenuated under high ionic strength, indicating contributions from both aromatic and electrostatic interactions (Figure 6B, left). Supporting this, FUS RRM interaction sites map to aromatic-rich, and to a lesser extent arginine-rich, regions of CAPRIN1.

Notably, theses heterotypic client interaction regions in CAPRIN1 overlap with the same regions responsible for driving CAPRIN1 phase separation through homotypic scaffold-scaffold contacts,[17] suggesting a shared molecular basis for homotypic and heterotypic recognition in this case. Of interest, coarse-grained simulations of multicomponent condensates predict that unlike low-valency clients that compete for scaffold-scaffold binding sites, high-valency clients can bridge scaffold interactions, leading to their enrichment in condensates.[47] Our findings are consistent with this model; the high valence FUS RRM client partitions extensively within CAPRIN1 condensates (K_p = 29) under the conditions of our experiments (i.e., much lower concentration of FUS RRM than available interaction sites on the scaffold). Phosphorylation of CAPRIN1 tyrosine side chains, which simultaneously modulates the net charge of the CAPRIN1 chain and the chemical properties of the aromatic side chains, reduces FUS RRM partitioning by over 2 orders of magnitude. This highlights how post-translational modifications, such as phosphorylation, can dramatically alter condensate composition by disrupting

https://doi.org/10.1021/jacs.5c10918
J. Am. Chem. Soc. 2025, 147, 33071−33085

key molecular interactions, offering a tunable mechanism to regulate client recruitment within condensates. It is worth emphasizing that the partition coefficients reported in this study were measured on samples incubated at 0 °C, where the unfolded FUS RRM populations in both dilute and condensed phases are negligible (see above). Thus, the measured K_p values refer to the partitioning of folded proteins into the CAPRIN1 condensate.

We have previously shown that CAPRIN1 condensates unfold the FUS RRM domain, with populations of the unfolded state as high as 31% and 64% at 25 °C and 40 °C, respectively.[20] CAPRIN1 interactions with the unfolded state were found to include both hydrophobic and electrostatic contributions, in particular, involving Arg and aromatic residue side chains from the scaffold. The present study establishes that these residue types also participate in the partitioning of the folded FUS RRM inside condensates, where charge-based and aromatic interactions involving both molecular components are critical. However, on a more detailed level, the pattern of CAPRIN1 interactions with the unfolded FUS RRM conformers differs markedly from those observed here for the folded state. Specifically, intermolecular contacts involving the N-terminal negatively charged region (D276-T286), which are observed in the folded conformation are absent for the unfolded ensemble.[20] Instead, unfolded interaction sites are found in a region N-terminal to the α1 helix, which are uniquely accessible in the unfolded state. While we showed that these exposed sites in the unfolded state engage with CAPRIN1, in more complex condensates involving many more biomolecules, these sites may serve to recruit additional clients, adding a further layer of regulatory complexity. These observations suggest that CAPRIN1 engages different chemical groups and surfaces of FUS RRM depending on the client's conformational state, indicating a dynamic, conformation-dependent interaction landscape that may influence both client stability and partitioning within the condensate.

Our findings underscore the importance of structural context in dictating client partitioning into condensates, particularly for folded proteins whose interaction surfaces are defined by three-dimensional conformation rather than primary sequence alone. They also highlight the potential for complex regulatory mechanisms arising from conformational changes in clients, such as folding-unfolding transitions, which may differentially influence both condensate stability, in cases where contacts between clients and scaffolds compete with homotypic scaffolding interactions, and condensate composition. Moreover, our work showcases the dramatic impact of scaffold post-translational modifications on client recruitment. It is noteworthy that many scaffold proteins have significant numbers of sites that can be post-translationally modified,[48] resulting in changes to their chain properties and, hence, modulating their abilities to solvate client molecules. Dissecting how such modifications impact the interaction valence and network connectivity within condensates will be important for understanding cellular control over condensate dynamics. Combining residue-level structural information, as gathered from the NMR approaches described here, with computational modeling will help establish generalized principles linking surface chemistry, interaction valence, and condensate enrichment. Finally, efforts to integrate these atomistic details into predictive models, whether structure-based or machine-learning approaches, will be key for building a unified framework that accurately captures the molecular determinants of selective partitioning across both disordered and folded proteomes.

■ ASSOCIATED CONTENT

Supporting Information

The Supporting Information is available free of charge at https://pubs.acs.org/doi/10.1021/jacs.5c10918.

Protocol for preparation of phase-separated NMR sample, supporting data for client-scaffold interaction maps and mass spectrometry characterization of CAPRIN1 phosphorylation (PDF)

■ AUTHOR INFORMATION

Corresponding Authors

Rashik Ahmed − *Department of Molecular Genetics, University of Toronto, Toronto, ON M5S 1A8, Canada; Department of Chemistry, University of Toronto, Toronto, ON M5S 3H6, Canada; Department of Biochemistry, University of Toronto, Toronto, ON M5S 1A8, Canada; Program in Molecular Medicine, Hospital for Sick Children Research Institute, Toronto, ON M5G 0A4, Canada*; Email: ahmedrt1994@gmail.com

Lewis E. Kay − *Department of Molecular Genetics, University of Toronto, Toronto, ON M5S 1A8, Canada; Department of Chemistry, University of Toronto, Toronto, ON M5S 3H6, Canada; Department of Biochemistry, University of Toronto, Toronto, ON M5S 1A8, Canada; Program in Molecular Medicine, Hospital for Sick Children Research Institute, Toronto, ON M5G 0A4, Canada*; orcid.org/0000-0002-4054-4083; Email: lewis.kay@utoronto.ca

Authors

Jeffrey P. Bonin − *Department of Molecular Genetics, University of Toronto, Toronto, ON M5S 1A8, Canada; Department of Chemistry, University of Toronto, Toronto, ON M5S 3H6, Canada; Department of Biochemistry, University of Toronto, Toronto, ON M5S 1A8, Canada*

Julie D. Forman-Kay − *Department of Biochemistry, University of Toronto, Toronto, ON M5S 1A8, Canada; Program in Molecular Medicine, Hospital for Sick Children Research Institute, Toronto, ON M5G 0A4, Canada*; orcid.org/0000-0001-8265-972X

Complete contact information is available at: https://pubs.acs.org/10.1021/jacs.5c10918

Notes

The authors declare no competing financial interest.

■ ACKNOWLEDGMENTS

R.A. is grateful for a Restracomp postdoctoral fellowship from the Research Institute of the Hospital for Sick Children. L.E.K. acknowledges support from the Canadian Institutes of Health Research (CIHR) (FND-503573) and the Natural Sciences and Engineering Council of Canada (024-03872). J.D.F.-K. acknowledges support from the CIHR (PJT-190060), the Natural Sciences and Engineering Council of Canada (NSERC) (2024-05725), and from the Canada Research Chairs Program.

REFERENCES

(1) Banani, S. F.; Lee, H. O.; Hyman, A. A.; Rosen, M. K. Biomolecular Condensates: Organizers of Cellular Biochemistry. *Nat. Rev. Mol. Cell Biol.* **2017**, *18* (5), 285−298.

(2) Shin, Y.; Brangwynne, C. P. Liquid Phase Condensation in Cell Physiology and Disease. *Science* **2017**, *357* (6357), No. eaaf4382.

(3) Choi, J. M.; Holehouse, A. S.; Pappu, R. V. Physical Principles Underlying the Complex Biology of Intracellular Phase Transitions. *Annu. Rev. Biophys* **2020**, *49*, 107−133.

(4) Mittag, T.; Pappu, R. V. A Conceptual Framework for Understanding Phase Separation and Addressing Open Questions and Challenges. *Mol. Cell* **2022**, *82* (12), 2201−2214.

(5) Ahmed, R.; Liang, M.; Hudson, R. P.; Rangadurai, A. K.; Huang, S. K.; Forman-Kay, J. D.; Kay, L. E. Atomic Resolution Map of the Solvent Interactions Driving SOD1 Unfolding in CAPRIN1 Condensates. *Proc. Natl. Acad. Sci.U.S.A.* **2024**, *121* (35), No. e2408554121.

(6) Peeples, W.; Rosen, M. K. Mechanistic Dissection of Increased Enzymatic Rate in a Phase Separated Compartment. *Nat. Chem. Biol.* **2021**, *17* (6), 693.

(7) Tibble, R. W.; Depaix, A.; Kowalska, J.; Jemielity, J.; Gross, J. D. Biomolecular Condensates Amplify MRNA Decapping by Biasing Enzyme Conformation. *Nat. Chem. Biol.* **2021**, *17* (5), 615.

(8) Ditlev, J. A.; Case, L. B.; Rosen, M. K. Who's In and Who's Out—Compositional Control of Biomolecular Condensates. *J. Mol. Biol.* **2018**, *430* (23), 4666−4684.

(9) Sever, A. I. M.; Ahmed, R.; Rößler, P.; Kay, L. E. Solution NMR Goes Big: Atomic Resolution Studies of Protein Components of Molecular Machines and Phase-Separated Condensates. *Curr. Opin Struct Biol.* **2025**, *90*, No. 102976.

(10) Abyzov, A.; Blackledge, M.; Zweckstetter, M. Conformational Dynamics of Intrinsically Disordered Proteins Regulate Biomolecular Condensate Chemistry. *Chem. Rev.* **2022**, *122* (6), 6719−6748.

(11) Flores-Solis, D.; Lushpinskaia, I. P.; Polyansky, A. A.; Changiarath, A.; Boehning, M.; Mirkovic, M.; Walshe, J.; Pietrek, L. M.; Cramer, P.; Stelzl, L. S.; Zagrovic, B.; Zweckstetter, M. Driving Forces behind Phase Separation of the Carboxy-Terminal Domain of RNA Polymerase II. *Nat. Commun.* **2023**, *14* (1), No. 5979.

(12) Guseva, S.; Schnapka, V.; Adamski, W.; Maurin, D.; Ruigrok, R. W. H.; Salvi, N.; Blackledge, M. Liquid-Liquid Phase Separation Modifies the Dynamic Properties of Intrinsically Disordered Proteins. *J. Am. Chem. Soc.* **2023**, *145* (19), 10548−10563.

(13) Murthy, A. C.; Dignon, G. L.; Kan, Y.; Zerze, G. H.; Parekh, S. H.; Mittal, J.; Fawzi, N. L. Molecular Interactions Underlying Liquid-Liquid Phase Separation of the FUS Low Complexity Domain. *Nat. Struct Mol. Biol.* **2019**, *26* (7), 637−648.

(14) Toyama, Y.; Rangadurai, A. K.; Forman-Kay, J. D.; Kay, L. E. Mapping the Per-Residue Surface Electrostatic Potential of CAPRIN1 along Its Phase-Separation Trajectory. *Proc. Natl. Acad. Sci. U.S.A.* **2022**, *119* (36), No. e2210492119.

(15) Toyama, Y.; Rangadurai, A. K.; Forman-Kay, J. D.; Kay, L. E. Surface Electrostatics Dictate RNA-Binding Protein CAPRIN1 Condensate Concentration and Hydrodynamic Properties. *J. Biol. Chem.* **2023**, *299* (1), 299−300.

(16) Wong, L. E.; Kim, T. H.; Muhandiram, D. R.; Forman-Kay, J. D.; Kay, L. E. NMR Experiments for Studies of Dilute and Condensed Protein Phases: Application to the Phase-Separating Protein CAPRIN1. *J. Am. Chem. Soc.* **2020**, *142* (5), 2471−2489.

(17) Kim, T. H.; Payliss, B. J.; Nosella, M. L.; Lee, I. T. W.; Toyama, Y.; Forman-Kay, J. D.; Kay, L. E. Interaction Hot Spots for Phase Separation Revealed by NMR Studies of a CAPRIN1 Condensed Phase. *Proc. Natl. Acad. Sci. U.S.A.* **2021**, *118* (23), No. e2104897118.

(18) Murthy, A. C.; Tang, W. S.; Jovic, N.; Janke, A. M.; Seo, D. H.; Perdikari, T. M.; Mittal, J.; Fawzi, N. L. Molecular Interactions Contributing to FUS SYGQ LC-RGG Phase Separation and Co-Partitioning with RNA Polymerase II Heptads. *Nat. Struct. Mol. Biol.* **2021**, *28* (11), 923−935.

(19) Rangadurai, A. K.; Ruetz, L.; Ahmed, R.; Lo, K.; Tollinger, M.; Forman-Kay, J. D.; Kreutz, C.; Kay, L. E. Phase Separation Modulates the Thermodynamics and Kinetics of RNA Hybridization. *J. Am. Chem. Soc.* **2024**, *146*, 19686−19689.

(20) Ahmed, R.; Hudson, R. P.; Forman-Kay, J. D.; Kay, L. E. Client-Scaffold Interactions Suppress Aggregation of a Client Protein in Model Condensates *Proc. Natl. Acad. Sci. USA* 2025, *122*, e2508403122 DOI: 10.1073/pnas.2508403122.

(21) Ahmed, R.; Rangadurai, A. K.; Ruetz, L.; Tollinger, M.; Kreutz, C.; Kay, L. E. A Delayed Decoupling Methyl-TROSY Pulse Sequence for Atomic Resolution Studies of Folded Proteins and RNAs in Condensates. *J. Magn. Reson.* **2024**, *362*, No. 107667.

(22) Delaglio, F.; Grzesiek, S.; Vuister, G. W.; Zhu, G.; Pfeifer, J.; Bax, A. NMRPipe: A Multidimensional Spectral Processing System Based on UNIX Pipes. *J. Biomol. NMR* **1995**, *6* (3), 277−293.

(23) Lee, W.; Tonelli, M.; Markley, J. L. NMRFAM-SPARKY: Enhanced Software for Biomolecular NMR Spectroscopy. *Bioinformatics* **2015**, *31* (8), 1325−1327.

(24) Choy, W. Y.; Mulder, F. A. A.; Crowhurst, K. A.; Muhandiram, D. R.; Millett, I. S.; Doniach, S.; Forman-Kay, J. D.; Kay, L. E. Distribution of Molecular Size within an Unfolded State Ensemble Using Small-Angle X-Ray Scattering and Pulse Field Gradient NMR Techniques. *J. Mol. Biol.* **2002**, *316* (1), 101−112.

(25) Huang, R.; Brady, J. P.; Yuwen, T.; Sekhar, A.; Kay, L. E. An Enhanced Sensitivity Methyl (1)H Triple-Quantum Pulse Scheme for Measuring Diffusion Constants of Macromolecules. *J. Biomol. NMR* **2017**, *68* (4), 249−255.

(26) Kim, T. H.; Nosella, M. L.; Bolik-Coulon, N.; Harkness, R. W.; Huang, S. K.; Kay, L. E. Correlating Histone Acetylation with Nucleosome Core Particle Dynamics and Function. *Proc. Natl. Acad. Sci. U.S.A.* **2023**, *120* (15), No. e2301063120.

(27) Lakomek, N. A.; Ying, J.; Bax, A. Measurement of ^{15}N Relaxation Rates in Perdeuterated Proteins by TROSY-Based Methods. *J. Biomol. NMR* **2012**, *53* (3), 209−221.

(28) Palmer, A. G.; Kroenke, C. D.; Loria, J. P. Nuclear Magnetic Resonance Methods for Quantifying Microsecond-to-Millisecond Motions in Biological Macromolecules. *Methods Enzymol.* **2001**, *339*, 204−238.

(29) Ferrage, F.; Piserchio, A.; Cowburn, D.; Ghose, R. On the Measurement of 15N-{1H} Nuclear Overhauser Effects. *J. Magn. Reson.* **2008**, *192* (2), 302.

(30) Walker, O.; Varadan, R.; Fushman, D. Efficient and Accurate Determination of the Overall Rotational Diffusion Tensor of a Molecule from 15N Relaxation Data Using Computer Program ROTDIF. *J. Magn. Reson.* **2004**, *168* (2), 336−345.

(31) Kneller, J. M.; Lu, M.; Bracken, C. An Effective Method for the Discrimination of Motional Anisotropy and Chemical Exchange. *J. Am. Chem. Soc.* **2002**, *124* (9), 1852−1853.

(32) Mandel, A. M.; Akke, M.; Palmer, A. G. Backbone Dynamics of *Escherichia Coli* Ribonuclease HI: Correlations with Structure and Function in an Active Enzyme. *J. Mol. Biol.* **1995**, *246* (1), 144−163.

(33) Kaushik Rangadurai, A.; Toyama, Y.; Kay, L. E. Practical Considerations for the Measurement of Near-Surface Electrostatics Based on Solvent Paramagnetic Relaxation Enhancements. *J. Magn. Reson.* **2023**, *349*, No. 107400.

(34) Geen, H.; Freeman, R. Band-selective Radiofrequency pulses. *J. Magn. Reson.* **1991**, *93* (1), 93−141.

(35) Mateju, D.; Franzmann, T. M.; Patel, A.; Kopach, A.; Boczek, E. E.; Maharana, S.; Lee, H. O.; Carra, S.; Hyman, A. A.; Alberti, S. An Aberrant Phase Transition of Stress Granules Triggered by Misfolded Protein and Prevented by Chaperone Function. *EMBO J.* **2017**, *36* (12), 1669.

(36) Tugarinov, V.; Kay, L. E. An Isotope Labeling Strategy for Methyl TROSY Spectroscopy. *J. Biomol. NMR* **2004**, *28* (2), 165−172.

(37) Tugarinov, V.; Sprangers, R.; Kay, L. E. Probing Side-Chain Dynamics in the Proteasome by Relaxation Violated Coherence Transfer NMR Spectroscopy. *J. Am. Chem. Soc.* **2007**, *129* (6), 1743−1750.

(38) Song, X. J.; Flynn, P. F.; Sharp, K. A.; Wand, A. J. Temperature Dependence of Fast Dynamics in Proteins. *Biophys. J.* **2007**, *92* (6), L43−L45.
(39) *Biomolecular NMR tools - SSPPS NMR Facility - UC San Diego*. https://sopnmr.ucsd.edu/biomol-tools.htm (accessed May 24, 2025).
(40) Lyons, H.; Veettil, R. T.; Pradhan, P.; Fornero, C.; De La Cruz, N.; Ito, K.; Eppert, M.; Roeder, R. G.; Sabari, B. R. Functional Partitioning of Transcriptional Regulators by Patterned Charge Blocks. *Cell* **2023**, *186* (2), 327−345.e28.
(41) Pritišanac, I.; Alderson, T. R.; Kolarić, Đ.; Zarin, T.; Xie, S.; Lu, A.; Alam, A.; Maqsood, A.; Youn, J.-Y.; Forman-Kay, J. D.; Moses, A. M. A Functional Map of the Human Intrinsically Disordered Proteome. *bioRxiv* **2024**, DOI: 10.1101/2024.03.15.585291.
(42) Kilgore, H. R.; Chinn, I.; Mikhael, P. G.; Mitnikov, I.; Van Dongen, C.; Zylberberg, G.; Afeyan, L.; Banani, S. F.; Wilson-Hawken, S.; Lee, T. I.; Barzilay, R.; Young, R. A. Protein Codes Promote Selective Subcellular Compartmentalization. *Science* **2025**, *387* (6738), 1095−1101.
(43) Brady, J. P.; Farber, P. J.; Sekhar, A.; Lin, Y. H.; Huang, R.; Bah, A.; Nott, T. J.; Chan, H. S.; Baldwin, A. J.; Forman-Kay, J. D.; Kay, L. E. Structural and Hydrodynamic Properties of an Intrinsically Disordered Region of a Germ Cell-Specific Protein on Phase Separation. *Proc. Natl. Acad. Sci. U.S.A.* **2017**, *114* (39), E8194−E8203.
(44) Kim, T. H.; Tsang, B.; Vernon, R. M.; Sonenberg, N.; Kay, L. E.; Forman-Kay, J. D. Phospho-Dependent Phase Separation of FMRP and CAPRIN1 Recapitulates Regulation of Translation and Deadenylation. *Science* **2019**, *365* (6455), 825−829.
(45) Tugarinov, V.; Hwang, P. M.; Ollerenshaw, J. E.; Kay, L. E. Cross-Correlated Relaxation Enhanced 1H-13C NMR Spectroscopy of Methyl Groups in Very High Molecular Weight Proteins and Protein Complexes. *J. Am. Chem. Soc.* **2003**, *125* (34), 10420−10428.
(46) Segur, J. B.; Oderstar, H. E. Viscosity of Glycerol and Its Aqueous Solutions. *Ind. Eng. Chem.* **1951**, *43* (9), 2117−2120.
(47) Espinosa, J. R.; Joseph, J. A.; Sanchez-Burgos, I.; Garaizar, A.; Frenkel, D.; Collepardo-Guevara, R. Liquid Network Connectivity Regulates the Stability and Composition of Biomolecular Condensates with Many Components. *Proc. Natl. Acad. Sci. U.S.A.* **2020**, *117* (24), 13238−13247.
(48) Vernon, R. M. C.; Chong, P. A.; Tsang, B.; Kim, T. H.; Bah, A.; Farber, P.; Lin, H.; Forman-Kay, J. D. Pi-Pi Contacts Are an Overlooked Protein Feature Relevant to Phase Separation. *Elife* **2018**, *7*, No. e31486.
(49) Hebditch, M.; Warwicker, J. Web-Based Display of Protein Surface and PH-Dependent Properties for Assessing the Developability of Biotherapeutics. *Sci. Rep.* **2019**, *9* (1), No. 1969.